Citation for published version:
Raupp, CFM, Silva Dias, PL, Tabak, EG & Milewski, PA 2008, 'Resonant wave interactions in the equatorial waveguide', *Journal of the Atmospheric Sciences*, vol. 65, no. 11, pp. 3398-3418. https://doi.org/10.1175/2008JAS2387.1

DOI:
10.1175/2008JAS2387.1

Publication date:
2008

Link to publication

© Copyright 2008 American Meteorological Society (AMS). Permission to use figures, tables, and brief excerpts from this work in scientific and educational
works is hereby granted provided that the source is acknowledged. Any use of material in
this work that is determined to be “fair use” under Section 107 of the U.S. Copyright Act September 2010 Page 2
or that satisfies the conditions specified in Section 108 of the U.S. Copyright Act (17
USC §108, as revised by P.L. 94-553) does not require the AMS’s permission.
Republication, systematic reproduction, posting in electronic form, such as on a web site
or in a searchable database, or other uses of this material, except as exempted by the
above statement, requires written permission or a license from the AMS. Additional
details are provided in the AMS Copyright Policy, available on the AMS Web site
located at (http://www.ametsoc.org/) or from the AMS at 617-227-2425 or
copyright@ametsoc.org.

University of Bath

Alternative formats
If you require this document in an alternative format, please contact:
openaccess@bath.ac.uk

General rights
Copyright and moral rights for the publications made accessible in the public portal are retained by the authors and/or other copyright owners and it is a condition of accessing publications that users recognise and abide by the legal requirements associated with these rights.

Take down policy
If you believe that this document breaches copyright please contact us providing details, and we will remove access to the work immediately and investigate your claim.

Download date: 06. May. 2023

Resonant Wave Interactions in the Equatorial Waveguide

CARLOS F. M. RAUPP AND PEDRO L. SILVA DIAS
Department of Atmospheric Sciences, Institute of Astronomy, Geophysics and Atmospheric Sciences, University of São Paulo, São Paulo, Brazil

ESTEBAN G. TABAK
Courant Institute of Mathematical Sciences, New York University, New York, New York

PAUL MILEWSKI
Department of Mathematics, University of Wisconsin—Madison, Madison, Wisconsin

(Manuscript received 3 January 2007, in final form 24 March 2008)

ABSTRACT

Weakly nonlinear interactions among equatorial waves have been explored in this paper using the adiabatic version of the equatorial β-plane primitive equations in isobaric coordinates. Assuming rigid lid vertical boundary conditions, the conditions imposed at the surface and at the top of the troposphere were expanded in a Taylor series around two isobaric surfaces in an approach similar to that used in the theory of surface–gravity waves in deep water and capillary–gravity waves. By adopting the asymptotic method of multiple time scales, the equatorial Rossby, mixed Rossby–gravity, inertio-gravity, and Kelvin waves, as well as their vertical structures, were obtained as leading-order solutions. These waves were shown to interact resonantly in a triad configuration at the $O(\varepsilon)$ approximation. The resonant triads whose wave components satisfy a resonance condition for their vertical structures were found to have the most significant interactions, although this condition is not excluding, unlike the resonant conditions for the zonal wavenumbers and meridional modes. Thus, the analysis has focused on such resonant triads. In general, it was found that for these resonant triads satisfying the resonance condition in the vertical direction, the wave with the highest absolute frequency always acts as an energy source (or sink) for the remaining triad components, as usually occurs in several other physical problems in fluid dynamics. In addition, the zonally symmetric geostrophic modes act as catalyst modes for the energy exchanges between two dispersive waves in a resonant triad. The integration of the reduced asymptotic equations for a single resonant triad shows that, for the initial mode amplitudes characterizing realistic magnitudes of atmospheric flow perturbations, the modes in general exchange energy on low-frequency (intraseasonal and/or even longer) time scales, with the interaction period being dependent upon the initial mode amplitudes. Potential future applications of the present theory to the real atmosphere with the inclusion of diabatic forcing, dissipation, and a more realistic background state are also discussed.

1. Introduction

In the atmosphere, equatorially trapped wave motions constitute a prominent characteristic of the general circulation and play an important role in the climate. The phenomenon of the equator acting as a waveguide was theoretically discovered by Matsuno (1966), who derived a complete set of free linear wave-mode solutions of the shallow-water equations on the equatorial β plane. Since this theoretical finding, the linear theory of equatorial waves has been extensively generalized with the inclusion of forcing, dissipation, more realistic background flows, and parameterization of moist processes and boundary layer drag to explain fundamental features of tropical climate. Nevertheless, because the governing equations of the atmospheric motions are nonlinear, one would like to understand the effects of the nonlinearity on these equatorially trapped disturbances.

It is well known (Bretherton 1964; Ripa 1981, 1982, 1983a,b) that in the finite amplitude limit dispersive waves only interact effectively if they are resonant, that is, when they form three- or four-wave interactions with other modes of the system such that the wavenumbers and frequencies of the modes both add to zero. In this sense, any dispersive system having quadratic nonlinearities to lowest order may exhibit triad resonance phenomena as leading-order nonlinear effects. This in-

Corresponding author address: Carlos F. M. Raupp, Rua do Matão, 1226 Cidade Universitária, São Paulo, SP 05508-090, Brazil.
E-mail: cfmraupp@model.iag.usp.br

DOI: 10.1175/2008JAS2387.1

© 2008 American Meteorological Society

teresting phenomenon in nonlinear wave–wave interactions was noticed by Phillips (1960) while discussing the role of small nonlinear terms in the theory of ocean waves; it has then been applied to a wide range of problems in physics. A rich and complete discussion on resonant triad interaction among dispersive waves can be found in Bretherton (1964) in his analysis of a simple wave equation "forced" by a quadratic term. With regard to the equatorial atmospheric waves, most of the theoretical studies on their nonlinear dynamics are based on the shallow-water equations with the equatorial β-plane approximation. Domaracki and Loesch (1977) first studied resonant triads of equatorial waves using the asymptotic method of multiple scales; Loesch and Deininger (1979) extended Domaracki and Loesch's results for resonantly interacting waves in coupled triad configurations. Ripa (1982, 1983a,b) formulated the nonlinear wave–wave interaction problem in the equatorial waveguide by using Galerkin formalism with the basis functions given by the eigensolutions of the linear problem and showed that the conservation of two particular integrals of motion, quadratic to lowest order, leads to interesting properties that the coupling coefficients must satisfy to ensure the invariance of such integrals. Ripa (1982) applied this formalism to the Kelvin mode self-interactions and then (Ripa 1983a,b) studied the resonant triad interaction involving the dispersive waves. According to these studies, in the equatorial waveguide are resonant triads composed of the same as well as different wave types. In addition, a fundamental result of these studies is that in the resonant triads involving equatorial waves, the wave having the maximum absolute time frequency always acts as an energy source (or sink) for the remaining triad components, as usually occurs with the three-wave resonances in several other problems in fluid dynamics (see chapter 5 of Craik 1985 and references therein). Recently, Raupp and Silva Dias (2006) explored the dynamics of two resonant triads coupled by one mode and pointed out the importance of the highest absolute frequency modes in the resonant triads for intertriad energy exchanges.

Because the results mentioned above are based on the shallow-water equations, an important issue that arises from these studies is how the vertical stratification of the atmosphere influences the nonlinear interactions among equatorial waves. Previous studies of the linear equatorial wave theory in the fully stratified case (Silva Dias et al. 1983; DeMaria 1985) show that in the linear context the primitive equations with some kind of rigid lid vertical boundary conditions can be separable into the vertical structure equation and a series of shallow-water equations governing the time evolution of the horizontal structure associated with each vertical eigenmode. Thus, in the nonlinear case of the stratified model, equatorial waves associated with different vertical eigenmodes may interact resonantly. In this context, an important question is how the vertical structure of the waves and the vertical boundary conditions restrict the wave interactions in the equatorial waveguide. Therefore, to address this issue, in this paper we extend the previous results on the nonlinear interactions among equatorial waves to the fully stratified case. The nonlinear dynamical equations utilized here for this purpose are the equatorial β-plane primitive equations in isobaric coordinates. As will be shown later, the use of pressure as the vertical coordinate is suitable for our analysis method because of the linear character of both the continuity and the hydrostatic equations. To simplify the mathematical analysis, the resonant interactions will be analyzed in an idealized setting, with the waves embedded in a motionless, hydrostatic, horizontally homogeneous and stably stratified background atmosphere. Furthermore, because the emphasis is on the wave–wave energy exchanges caused by the nonlinear terms alone, other important physical processes in the atmosphere, such as diabatic effects and the boundary layer drag, are all omitted here for simplicity in exposition.

The reminder of this paper is organized as follows: In section 2, the asymptotic method of multiple time scales is applied to the governing equations to obtain an asymptotic reduced system of equations governing the weakly nonlinear interaction among the waves in a resonant triad. In section 3 we derive the total energy conservation of the leading-order solution to get some energy constraints that the waves must satisfy. In section 4, we analyze how the vertical structure of the waves restricts the resonant triad interactions. In addition, section 4 shows some examples of resonant triads that undergo the most significant interactions among the waves. Section 5 explores the dynamics of these interactions by solving the reduced asymptotic equations for selected resonant triads. Potential future applications of the present theory to the real atmosphere with the inclusion of diabatic forcing, dissipation, and a more realistic background state are discussed in section 6.

2. Model equations and solution method

In this work we consider a model governing equatorially trapped large-scale perturbations of dry tropospheric motions embedded in a motionless, hydrostatic, horizontally homogeneous and stably stratified background atmosphere. This model can be represented by the following adiabatic version of the primitive equations in isobaric coordinates with the equatorial β-plane approximation:

$$\frac{\partial u}{\partial t} + \varepsilon\left(u\frac{\partial u}{\partial x} + v\frac{\partial u}{\partial y} + F\omega\frac{\partial u}{\partial p}\right) - yv + \frac{\partial \phi}{\partial x} = 0, \tag{2.1a}$$

$$\frac{\partial v}{\partial t} + \varepsilon\left(u\frac{\partial v}{\partial x} + v\frac{\partial v}{\partial y} + F\omega\frac{\partial v}{\partial p}\right) + yu + \frac{\partial \phi}{\partial y} = 0, \tag{2.1b}$$

$$\frac{\partial u}{\partial x} + \frac{\partial v}{\partial y} + F\frac{\partial \omega}{\partial p} = 0, \quad \text{and,} \tag{2.1c}$$

$$\frac{\partial}{\partial t}\frac{\partial \phi}{\partial p} + \varepsilon\left[u\frac{\partial}{\partial x}\frac{\partial \phi}{\partial p} + v\frac{\partial}{\partial y}\frac{\partial \phi}{\partial p} + F\omega\frac{\partial^2 \phi}{\partial p^2} + \frac{F\omega}{p}(1-\kappa)\frac{\partial \phi}{\partial p}\right] + F\tilde{\overline{\sigma}}\omega = 0. \tag{2.1d}$$

In the equations above, $\varepsilon = \mathrm{Ro} = U/(\beta L^2)$ is the equivalent for the equatorial region of the Rossby number in midlatitudes; β is the equatorial Rossby parameter and is assumed here as a constant, $F = \Theta/\mathrm{Ro}$, where $\Theta = \Omega/(\beta L p_0)$; $\kappa = R/C_p$, with R and C_p the gas constant for dry air and the thermal capacity of dry air at constant pressure, respectively; and $\tilde{\overline{\sigma}} = \overline{\sigma} p_0{}^2/(\beta^2 L^4)$, where $\overline{\sigma}$ is the static stability parameter of the background atmosphere, given by

$$\overline{\sigma} = \frac{R}{p'}\left(\frac{R\overline{T}}{p' C_p} - \frac{d\overline{T}}{dp'}\right). \tag{2.2}$$

In (2.2), $\overline{T} = \overline{T}(p')$ represents the background temperature. The static stability parameter is positive for a stably stratified atmosphere and will be assumed here as a constant with its typical tropospheric value of $\overline{\sigma} = 2 \times 10^{-6}\ \mathrm{m^4\ s^2\ kg^{-2}}$. The equations in (2.1) are nondimensionalized using the following scaling rules:

$$\begin{aligned} (u', v') &\sim O(U)(u, v),\\ (x', y') &\sim O(L)(x, y),\\ t' &\sim O[1/(\beta L)]t,\\ p' &= O(p_0)p,\\ \omega' &\sim O(\Omega)\omega, \quad \text{and}\\ \phi' &= O(\beta L^2 U)\phi. \end{aligned} \tag{2.3}$$

The quantity ϕ in (2.1) is the geopotential perturbation, (u, v) are the velocity perturbations in the (x, y) coordinate directions, and $\omega = Dp/Dt$ is the vertical velocity in pressure coordinates. Periodic solutions in the x direction and bounded solutions as $|y|$ tends to infinity represent the horizontal boundary conditions for our model. As vertical boundary conditions for system (2.1) we have assumed rigid lid boundary conditions such that the actual vertical velocity $w = (1/g)D\phi/Dt$ vanishes at $z = 0$ (the earth's surface) and at a finite top $z = z_T$ of the troposphere. This is a simplified model for the dynamical behavior of equatorially trapped large-scale motions in the troposphere in which both the coupling with the boundary layer and the coupling with the stratosphere are ignored. However, recently Haertel and Kiladis (2004) analyzed the dynamics of 2-day equatorial waves and demonstrated that, in this context, the rigid lid approximation with the top boundary located around 150 hPa is an excellent one for capturing the dynamical behavior of the waves in the troposphere, except in the regions close to the top (above 200 hPa) and to the surface (below 900 hPa). For this reason, complete fidelity of the model developed below is only expected outside of these regions. Nevertheless, a difficulty emerges when adopting these vertical boundary conditions in pressure coordinates because in an arbitrary perturbed state of model (2.1) the isobaric surfaces no longer coincide with z surfaces. The z surfaces are parallel to isobaric surfaces only at the unperturbed state, that is, when $u' = v' = \omega' = \phi' = 0$ and the total state of the atmosphere coincides with the background. However, because this work focuses on small-amplitude waves, the surface and the hypothetical top of the troposphere are close to the isobaric surfaces represented by p_0 and p_T, respectively, so the geopotential and pressure at the surface and at the top can be related to each other by the following Taylor expansions:

$$\phi_{\mathrm{tot}}(z = 0) = 0 = \overline{\phi}(p_0) + \phi'(x', y', p_0, t') + \left.\frac{d\overline{\phi}}{dp'}\right|_{p'=p_0}[p'(z = 0) - p_0] + \mathrm{TSO}, \tag{2.4a}$$

$$\phi_{\mathrm{tot}}(z = z_T) = \overline{\phi}(p_T) + \phi'(x', y', p_T, t') + \left.\frac{d\overline{\phi}}{dp'}\right|_{p'=p_T}[p_T - p'(z = z_T)] + \mathrm{TSO}, \tag{2.4b}$$

where TSO represents terms of secondary order, $\phi_{\mathrm{tot}} = \overline{\phi} + \phi'$, $p'(z = 0) = p'(x', y', z = 0, t')$, and $p'(z = z_T) = p'(x', y', z = z_T, t')$ correspond to the pressures at the surface and the top, respectively, and

p_0 and p_T represent the isobaric surfaces close to them. Disregarding the terms of secondary order (TSO) in (2.4), the vertical boundary conditions can be expressed as follows:

$$w[x', y', p_0 + \overline{\rho_0}\phi'(x', y', p_0, t'), t'] = 0 \quad \text{and} \tag{2.5a}$$

$$w[x', y', p_T - \overline{\rho_T}\phi'(x', y', p_T, t'), t'] = 0, \tag{2.5b}$$

where $\overline{\rho_0} = \overline{\rho}(p_0)$ and $\overline{\rho_T} = \overline{\rho}(p_T)$ are the background densities at the surface and at the top, respectively. The equation above assumes that the basic state satisfies both the hydrostatic equilibrium and the law of the ideal gas, that is, $d\overline{\phi}/dp' = -\overline{\rho}^{-1}$. Performing a Taylor expansion on Eqs. (2.5a) and (2.5b) around $p' = p_0$ and $p' = p_T$, respectively, substituting the expression

$$w = \frac{1}{g}\frac{D\phi'}{Dt'} = \frac{1}{g}\left(\frac{\partial\phi'}{\partial t'} + u'\frac{\partial\phi'}{\partial x'} + \upsilon'\frac{\partial\phi'}{\partial y'} + \omega'\frac{\partial\phi'}{\partial p'} + \omega'\frac{d\overline{\phi}}{dp'}\right)$$

into the resulting equations and scaling the final expression according to (2.3), we get

$$\frac{\partial\phi}{\partial t} + \varepsilon\left(u\frac{\partial\phi}{\partial x} + \upsilon\frac{\partial\phi}{\partial y} + F\omega\frac{\partial\phi}{\partial p}\right) - \frac{F\omega}{\tilde{\overline{\rho}}_0} + \varepsilon\,\tilde{\overline{\rho}}_0\phi(x, y, 1, t)\frac{\partial}{\partial p}\left[\frac{\partial\phi}{\partial t} + \varepsilon\left(u\frac{\partial\phi}{\partial x} + \upsilon\frac{\partial\phi}{\partial y} + F\omega\frac{\partial\phi}{\partial p}\right) - \frac{F\omega}{\tilde{\overline{\rho}}}\right] = 0, \text{ at } p = 1, \quad \text{and} \tag{2.6a}$$

$$\frac{\partial\phi}{\partial t} + \varepsilon\left(u\frac{\partial\phi}{\partial x} + \upsilon\frac{\partial\phi}{\partial y} + F\omega\frac{\partial\phi}{\partial p}\right) - \frac{F\omega}{\tilde{\overline{\rho}}_T} - \varepsilon\,\tilde{\overline{\rho}}_T\phi(x, y, \tilde{p}_T, t)\frac{\partial}{\partial p}\left[\frac{\partial\phi}{\partial t} + \varepsilon\left(u\frac{\partial\phi}{\partial x} + \upsilon\frac{\partial\phi}{\partial y} + F\omega\frac{\partial\phi}{\partial p}\right) - \frac{F\omega}{\tilde{\overline{\rho}}}\right] = 0, \text{ at } p = \tilde{p}_T, \tag{2.6b}$$

where $\tilde{p}_T = p_T/p_0$ and $\tilde{\overline{\rho}} = \overline{\rho}\beta^2L^4/p_0$. The Taylor expansion adopted here to solve the vertical boundary condition problem in isobaric coordinates is similar to that used in the theory of surface-gravity waves in deep water (Milewski and Keller 1996) and gravity–capillary waves (Case and Chiu 1977; McGoldrick 1965). Equations (2.1c) and (2.1d) can be combined to give

$$\frac{\partial}{\partial t}\frac{\partial}{\partial p}\left(\frac{1}{\tilde{\overline{\sigma}}}\frac{\partial\phi}{\partial p}\right) + \varepsilon\frac{\partial}{\partial p}\left[\frac{u}{\tilde{\overline{\sigma}}}\frac{\partial}{\partial x}\frac{\partial\phi}{\partial p} + \frac{\upsilon}{\tilde{\overline{\sigma}}}\frac{\partial}{\partial y}\frac{\partial\phi}{\partial p} + \frac{F\omega}{\tilde{\overline{\sigma}}}\frac{\partial^2\phi}{\partial p^2} + \frac{F\omega}{\tilde{\overline{\sigma}}p}(1-\kappa)\frac{\partial\phi}{\partial p}\right] - \left(\frac{\partial u}{\partial x} + \frac{\partial\upsilon}{\partial y}\right) = 0. \tag{2.7}$$

The nonlinear problem posed by (2.1a), (2.1b), (2.6), and (2.7) may be expanded in terms of the dimensionless parameter ε, which is a measure of the magnitude of the nonlinear products. Considering the typical magnitudes of large-scale perturbations in the atmosphere—$U \sim 5\ \text{m s}^{-1}$, $L \sim 1500$ km, and $\beta \sim 2.3 \times 10^{-11}\ \text{m}^{-1}\ \text{s}^{-1}$—it follows that $\varepsilon \sim 0.09$ and, as a consequence, a weakly nonlinear asymptotic analysis seems suitable for (2.1), (2.6), and (2.7). Therefore, assuming that (i) $0 < \varepsilon \ll 1$ and (ii) $F = O(1)$,[1] the procedure to be used here is the method of multiple time scales. It assumes a separation of a short time scale t and a long time scale represented by $\tau = \varepsilon t$. Formally, we allow all the dependent variables in (2.1), (2.6), and (2.7) to be functions of both time scales, and the separation is incorporated into these equations by the time-derivative transformation

$$\frac{\partial}{\partial t} \to \frac{\partial}{\partial t} + \varepsilon\frac{\partial}{\partial\tau}. \tag{2.8}$$

The dependent variables in (2.1) are also assumed to have uniformly valid asymptotic expansions of the forms

$$\begin{aligned} u &= u^{(0)}(x, y, p, t, \varepsilon t) + \varepsilon u^{(1)}(x, y, p, t, \varepsilon t) + O(\varepsilon^2),\\ \upsilon &= \upsilon^{(0)}(x, y, p, t, \varepsilon t) + \varepsilon\upsilon^{(1)}(x, y, p, t, \varepsilon t) + O(\varepsilon^2),\\ \phi &= \phi^{(0)}(x, y, p, t, \varepsilon t) + \varepsilon\phi^{(1)}(x, y, p, t, \varepsilon t) + O(\varepsilon^2), \quad \text{and}\\ \omega &= \omega^{(0)}(x, y, p, t, \varepsilon t) + \varepsilon\omega^{(1)}(x, y, p, t, \varepsilon t) + O(\varepsilon^2). \end{aligned} \tag{2.9}$$

Substituting the asymptotic expansions (2.8) and (2.9) into the governing equations (2.1a), (2.1b), (2.6), and (2.7), it follows that the leading-order solution is written according to

[1] In reality, assumption (ii) is not necessary for an asymptotic perturbation theory, but is needed to allow all the possible waves to represent the leading-order solution. This assumption is also based upon the uniformly occurrence of $O(\varepsilon)$ nonlinear terms in (2.1), (2.6), and (2.7) and the desire to mach anticipated nonlinear forcings with long time scale in the same power of ε.

$$\begin{bmatrix} u^{(0)}(x,y,p,t,\tau) \\ v^{(0)}(x,y,p,t,\tau) \\ \phi^{(0)}(x,y,p,t,\tau) \end{bmatrix} = \sum_a A_a(\tau)\xi_a(y)e^{ik_a x + i\varpi_a t}G_a(p) + \text{c.c.}, \tag{2.10}$$

where c.c. denotes the complex conjugate of the previous term. In (2.10), the subscript $a = (m, k, n, r)$ refers to a particular expansion mode characterized by a vertical mode m, a zonal wavenumber k, a meridional mode n distinguishing the meridional structure of the eigenfunctions $\xi_a(y)$, and the wave type r: $r = 1$ for Rossby waves (RWs), $r = 2$ for westward-propagating inertio-gravity waves (WGWs), and $r = 3$ for eastward-propagating inertio-gravity waves (EGWs). The mixed Rossby–gravity waves (MRGWs) are associated with the $n = 0$ mode and are included in the $r = 1$ (for $k > 2^{-1/2}$) and $r = 2$ (for $k < 2^{-1/2}$) categories. The Kelvin waves are represented by $n = -1$ and $r = 3$. In the leading-order solution represented by (2.10) are also degenerate eigenmodes associated with the eigenfrequency $\varpi = 0$. These modes have a $k = 0$ zonal structure and are characterized by a perfect geostrophic balance and the absence of a meridional circulation ($v = 0$) (Silva Dias and Schubert 1979). The $k = 0$ Kelvin modes are also included in this category. In (2.10), $G_a(p)$ represents the vertical structure functions that distinguish the vertical structure of the linear eigenmodes. These vertical structure functions are the eigenfunctions of the following Sturm–Liouville problem:

$$\frac{d}{dp}\left(\frac{1}{\tilde{\bar{\sigma}}}\frac{dG}{dp}\right) + \frac{1}{c^2}G = 0 \quad \text{and} \tag{2.11a}$$

$$\frac{dG}{dp} + \tilde{\bar{\sigma}}\tilde{\bar{\rho}}G = 0 \text{ at } p = 1 \quad \text{and} \quad \text{at } p = \tilde{p}_T, \tag{2.11b}$$

where c is the separation constant. If we further assume that the static stability parameter $\tilde{\bar{\sigma}}$ is constant with pressure, the eigenfunctions $G_m(p)$ are given by a combination of sines and cosines and the eigenvalues $\lambda_m = \sqrt{\tilde{\bar{\sigma}}}/c_m$ are determined by the following transcendental equation:

$$\lambda^2 \sin[(1-\tilde{p}_T)\lambda] - \lambda\,\tilde{\bar{\sigma}}(\tilde{\bar{\rho}}_0 - \tilde{\bar{\rho}}_T)\cos[(1-\tilde{p}_T)\lambda] + \tilde{\bar{\sigma}}^2\tilde{\bar{\rho}}_T\tilde{\bar{\rho}}_0\sin[(1-\tilde{p}_T)\lambda] = 0. \tag{2.12}$$

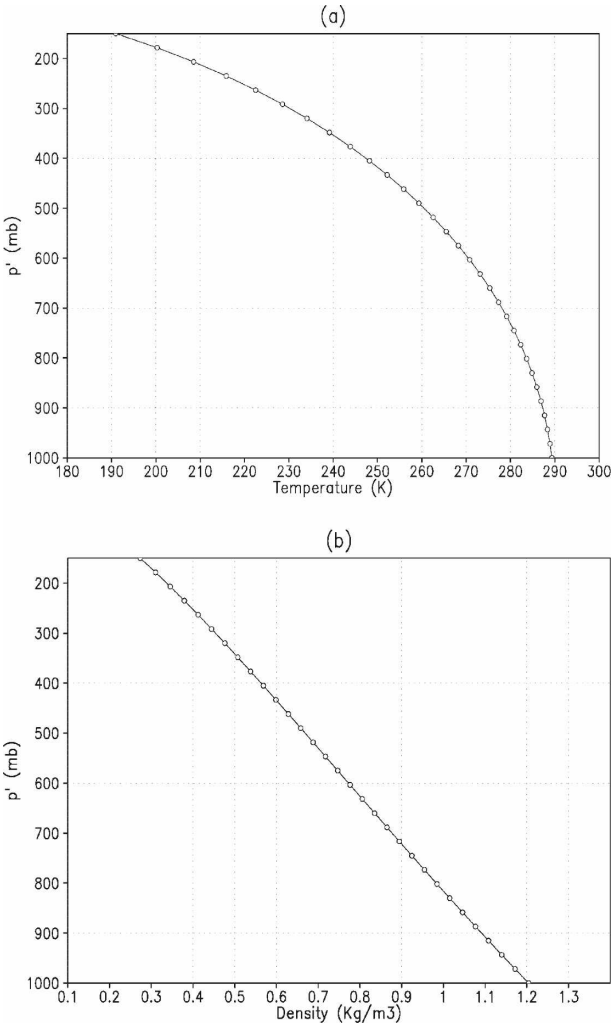

FIG. 1. (a) Background temperature $\overline{T}(p')$ and (b) density $\overline{\rho}(p')$ profiles used in this work for $\overline{\sigma} = 2 \times 10^{-6}$ m^4 s^2 kg^{-2}.

Figure 1 shows the basic state temperature and density profiles adopted in this work obtained by setting $\overline{\sigma} = 2 \times 10^{-6}$ m^4 s^2 kg^{-2}. The eigenvalues of the vertical structure equation obtained from the same value of the static stability parameter and for $L = 1.5 \times 10^6$ m, $p_0 = 1000$ hPa, and $p_T = 150$ hPa by using an iterative method are shown in Table 1. Table 1 also shows the separation constants c_m obtained from these eigenvalues. The eigenfunctions $G_m(p)$ associated with the eigenvalues λ_m shown in Table 1 are illustrated in Fig. 2. Because the eigenvalue $\lambda = 0$ is not physical, the $m = 0$ mode is associated with the first $\lambda \neq 0$ root of (2.12) and corresponds to the barotropic mode because its eigenfunction has no phase inversion and is almost constant throughout the troposphere. The $m > 0$ modes are usually referred to as internal or baroclinic modes and correspond to the oscillations associated with the rigid lid boundary conditions.

TABLE 1. Eigenvalues λ_m of the vertical structure Eq. (2.11), c_m, and $c_m\beta L^2$ (with $\beta = 2.3 \times 10^{-11}$ m^{-1} s^{-1} and $L = 1500$ km) for the first five vertical eigenmodes, $m = 0, 1, 2, 3$, and 4, for $p_0 = 1000$ hPa, $p_T = 150$ hPa, $\bar{\sigma} = 2 \times 10^{-6}$ m^4 s^2 kg^{-2}, and the profile $\bar{\rho}(p)$ shown in Fig. 1.

m	λ_m (dimensionless)	c_m (dimensionless)	$c_m\beta L^2$ (m s^{-1})
0	0.442	6.228	319.96
1	3.754	0.733	37.67
2	7.421	0.371	19.05
3	11.108	0.248	12.73
4	14.799	0.186	9.56

The meridional structure functions $\boldsymbol{\xi}_a(y) = [u_a(y), v_a(y), \phi_a(y)]^{\mathrm{T}}$ are given by a combination of Hermite functions and form an orthogonal and complete set at $(-\infty, +\infty)$ (Matsuno 1966). The finite-amplitude correction of the leading-order solution (2.10) is obtained from the $O(\varepsilon)$ problem, which is governed by the linear and inhomogeneous system

$$\Im\boldsymbol{\xi}^{(1)} = \mathbf{N}^{(0)}, \tag{2.13}$$

with the vertical boundary conditions expressed according to

$$\frac{\partial\phi^{(1)}}{\partial t} - \frac{F\omega^{(1)}}{\tilde{\bar{\rho}}_0} = -\left[\frac{\partial\phi^{(0)}}{\partial\tau} + u^{(0)}\frac{\partial\phi^{(0)}}{\partial x} + v^{(0)}\frac{\partial\phi^{(0)}}{\partial y} + F\omega^{(0)}\frac{\partial\phi^{(0)}}{\partial p} + \tilde{\bar{\rho}}_0\phi^{(0)}\frac{\partial}{\partial p}\left(\frac{\partial\phi^{(0)}}{\partial t} - \frac{F\omega^{(0)}}{\tilde{\bar{\rho}}}\right)\right] \text{ at } p = 1, \quad \text{and} \tag{2.14a}$$

$$\frac{\partial\phi^{(1)}}{\partial t} - \frac{F\omega^{(1)}}{\tilde{\bar{\rho}}_T} = -\left[\frac{\partial\phi^{(0)}}{\partial\tau} + u^{(0)}\frac{\partial\phi^{(0)}}{\partial x} + v^{(0)}\frac{\partial\phi^{(0)}}{\partial y} + F\omega^{(0)}\frac{\partial\phi^{(0)}}{\partial p} - \tilde{\bar{\rho}}_T\phi^{(0)}\frac{\partial}{\partial p}\left(\frac{\partial\phi^{(0)}}{\partial t} - \frac{F\omega^{(0)}}{\tilde{\bar{\rho}}}\right)\right] \text{ at } p = \tilde{p}_T. \tag{2.14b}$$

In (2.13), $\xi^{(1)} = [u^{(1)}, v^{(1)}, \phi^{(1)}]^{\mathrm{T}}$, $\Im$ is the linear operator given by

$$\Im = \begin{bmatrix} \dfrac{\partial}{\partial t} & -y & \dfrac{\partial}{\partial x} \\ y & \dfrac{\partial}{\partial t} & \dfrac{\partial}{\partial y} \\ -\dfrac{\partial}{\partial x} & -\dfrac{\partial}{\partial y} & \dfrac{\partial}{\partial t}\dfrac{\partial}{\partial p}\left(\dfrac{1}{\tilde{\bar{\sigma}}}\dfrac{\partial}{\partial p}\right) \end{bmatrix}, \tag{2.15}$$

and the vector $\mathbf{N}^{(0)}$ contains the leading-order contribution of the nonlinear terms in the governing Eqs. (2.1a, b) and (2.7) and the long-time evolution of $u^{(0)}$, $v^{(0)}$, and $\phi^{(0)}$. The inhomogeneous terms in (2.13) and (2.14) can potentially act as resonant forcings generating secular terms in $\xi^{(1)}$. As a consequence, to ensure that solution (2.10) represents the leading-order behavior formally, these secular solutions are required to vanish. This is achieved by the following solvability condition:

$$\lim_{\chi\to\infty}\frac{1}{2\chi\tilde{L}_x}\int_0^{\chi}\int_{-\tilde{L}_x}^{\tilde{L}_x}\int_{\tilde{p}_T}^{1}\langle\Im\boldsymbol{\xi}^{(1)}\cdot\boldsymbol{\xi}_a^{+}(y)e^{-ik_a x - i\varpi_a t}G_a(p)\rangle\,dp\,dx\,dt$$
$$= \lim_{\chi\to\infty}\frac{1}{2\chi\tilde{L}_x}\int_0^{\chi}\int_{-\tilde{L}_x}^{\tilde{L}_x}\int_{\tilde{p}_T}^{1}\langle\mathbf{N}^{(0)}\cdot\boldsymbol{\xi}_a^{+}(y)e^{-ik_a x - i\varpi_a t}G_a(p)\rangle\,dp\,dx\,dt, \tag{2.16}$$

with the inner product $\langle\cdot\rangle$ being defined by

$$\langle\mathbf{f}\cdot\mathbf{g}\rangle = \int_{-\infty}^{\infty}[f_1 g_1^* + f_2 g_2^* + f_3 g_3^*]\,dy, \tag{2.17}$$

where $\mathbf{f}$ and $\mathbf{g}$ are arbitrary vector functions satisfying the meridional boundary conditions of our problem, the subscripts 1, 2, and 3 refer to their scalar components, and the superscript * indicates the complex conjugate. In (2.16), $\tilde{L}_x$ represents the dimensionless zonal period defined by $\tilde{L}_x = 2\pi a_T/L$, with a_T representing the earth's radius; $\boldsymbol{\xi}_a^{+}(y)e^{-ik_a x - i\varpi_a t}G_a(p)$ represents an arbitrary null vector of the adjoint operator of $\Im$, where the meridional structure function $\boldsymbol{\xi}_a^{+}(y)$ can be written in terms of the meridional structure functions of the original $O(1)$ problem according to

$$\boldsymbol{\xi}_a^{+}(y) = \begin{bmatrix} u_a(y) \\ v_a^*(y) \\ -\phi_a(y) \end{bmatrix}. \tag{2.18}$$

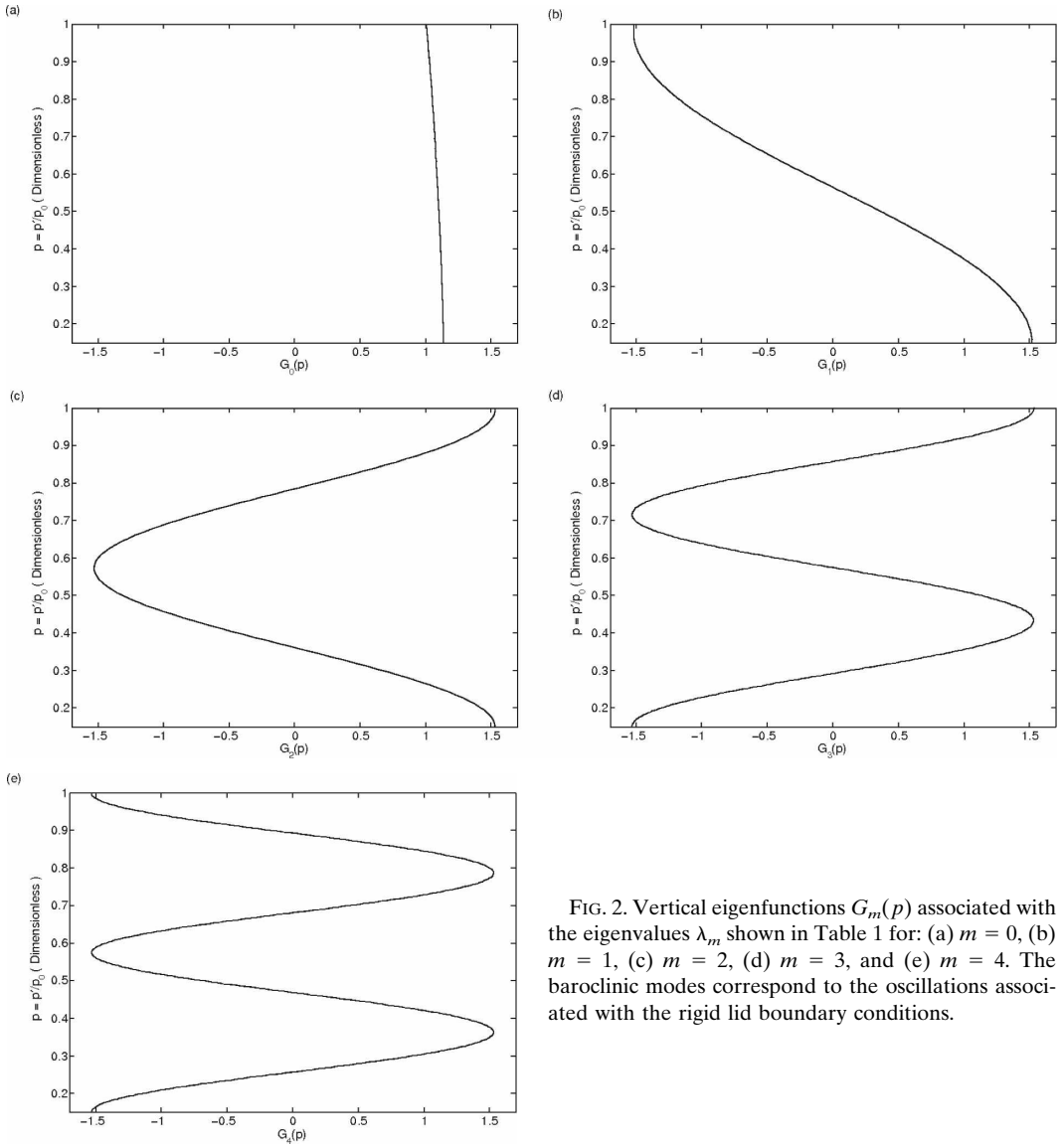

FIG. 2. Vertical eigenfunctions $G_m(p)$ associated with the eigenvalues λ_m shown in Table 1 for: (a) $m = 0$, (b) $m = 1$, (c) $m = 2$, (d) $m = 3$, and (e) $m = 4$. The baroclinic modes correspond to the oscillations associated with the rigid lid boundary conditions.

Integrating by parts the left-hand side of (2.16), using (2.11b) and the horizontal boundary conditions, and recalling that $\boldsymbol{\xi}_a^+(y)e^{-ik_a x - i\varpi_a t}G_a(p)$ satisfies the adjoint $O(1)$ problem, it follows that the solvability condition (2.16) can be expressed by

$$\lim_{\chi\to\infty}\frac{1}{2\chi\tilde{L}_x}\int_{-\tilde{L}_x}^{\tilde{L}_x}\int_{-\infty}^{+\infty}\int_0^{\chi}\left[\frac{1}{\tilde{\bar{\sigma}}}\phi_a^+(y)e^{-ik_a x}e^{-i\varpi_a t}G_a(p)\left(\frac{\partial}{\partial p}\frac{\partial\phi^{(1)}}{\partial t}+\tilde{\bar{\sigma}}\tilde{\bar{\rho}}\frac{\partial\phi^{(1)}}{\partial t}\right)\right]\Bigg|_{\tilde{p}_T}^{1}dt\,dy\,dx$$

$$=\lim_{\chi\to\infty}\frac{1}{2\chi\tilde{L}_x}\int_0^{\chi}\int_{-\tilde{L}_x}^{\tilde{L}_x}\int_{\tilde{p}_T}^{1}\langle\mathbf{N}^{(0)}\cdot\boldsymbol{\xi}_a^+(y)e^{-ik_a x-i\varpi_a t}G_a(p)\rangle\,dp\,dx\,dt. \tag{2.19}$$

On the other hand, the thermodynamics equation for $O(\varepsilon)$ is written as

$$\frac{\partial}{\partial t}\frac{\partial\phi^{(1)}}{\partial p}+\frac{\partial}{\partial\tau}\frac{\partial\phi^{(0)}}{\partial p}+u^{(0)}\frac{\partial}{\partial x}\frac{\partial\phi^{(0)}}{\partial p}+v^{(0)}\frac{\partial}{\partial y}\frac{\partial\phi^{(0)}}{\partial p}+F\omega^{(0)}\frac{\partial^2\phi^{(0)}}{\partial p^2}+\frac{F\omega^{(0)}}{p}(1-\kappa)\frac{\partial\phi^{(0)}}{\partial p}+F\tilde{\bar{\sigma}}\omega^{(1)}=0. \tag{2.20}$$

Thus, combining (2.20) and (2.14) and using both the continuity equation and the vertical boundary conditions of the leading-order solutions, it is possible to rewrite (2.19) as

$$\lim_{\chi\to\infty}\frac{1}{2\chi\tilde{L}_x}\int_{-\tilde{L}_x}^{\tilde{L}_x}\int_{-\infty}^{+\infty}\int_0^{\chi}\left\{\phi_a^+(y)e^{-ik_a x}e^{-i\varpi_a t}G_a(p)\left[-\tilde{\tilde{\rho}}\frac{\partial\phi^{(0)}}{\partial t}\frac{1}{\tilde{\tilde{\sigma}}}\frac{\partial^2\phi^{(0)}}{\partial p^2}+\tilde{\tilde{\Gamma}}\phi^{(0)}\frac{\partial\phi^{(0)}}{\partial t}-\Lambda\tilde{\tilde{\rho}}\phi^{(0)}\left(\frac{\partial u^{(0)}}{\partial x}+\frac{\partial v^{(0)}}{\partial y}\right)\right]\right\}\Bigg|_{\tilde{p}_T}^{1}dt\,dy\,dx$$

$$=\lim_{\chi\to\infty}\frac{1}{2\chi\tilde{L}_x}\int_0^{\chi}\int_{-\tilde{L}_x}^{\tilde{L}_x}\int_{\tilde{p}_T}^{1}\langle\mathbf{N}^{(0)}\cdot\boldsymbol{\xi}_a^+(y)e^{-ik_a x-i\varpi_a t}G_a(p)\rangle\,dp\,dx\,dt, \tag{2.21}$$

where $\tilde{\tilde{\Gamma}}=((1-\kappa)/p)\tilde{\tilde{\rho}}^2+\tilde{\tilde{\sigma}}\tilde{\tilde{\rho}}^3(1+\Lambda)-\Lambda\tilde{\tilde{\rho}}(d\tilde{\tilde{\rho}}/dp)$ and Λ is defined according to

$$\Lambda=\begin{cases}1, & if \quad p=1\\ -1, & if \quad p=\tilde{p}_T.\end{cases} \tag{2.22}$$

In (2.21), the vector $\mathbf{N}^{(0)}$ is expressed as

$$\mathbf{N}^{(0)=}[N_1,N_2,N_3]^{\mathrm{T}}, \tag{2.23a}$$

with the scalar components defined according to

$$N_1=-\frac{\partial u^{(0)}}{\partial\tau}-u^{(0)}\frac{\partial u^{(0)}}{\partial x}-v^{(0)}\frac{\partial u^{(0)}}{\partial y}-\tilde{\tilde{\rho}}_T\frac{\partial\phi^{(0)}}{\partial t}\Bigg|_{p=\tilde{p}_T}\frac{\partial u^{(0)}}{\partial p}+\int_{\tilde{p}_T}^{p}\left(\frac{\partial u^{(0)}}{\partial x}+\frac{\partial v^{(0)}}{\partial y}\right)dp\,\frac{\partial u^{(0)}}{\partial p}, \tag{2.23b}$$

$$N_2=-\frac{\partial v^{(0)}}{\partial\tau}-u^{(0)}\frac{\partial v^{(0)}}{\partial x}-v^{(0)}\frac{\partial v^{(0)}}{\partial y}-\tilde{\tilde{\rho}}_T\frac{\partial\phi^{(0)}}{\partial t}\Bigg|_{p=\tilde{p}_T}\frac{\partial v^{(0)}}{\partial p}+\int_{\tilde{p}_T}^{p}\left(\frac{\partial u^{(0)}}{\partial x}+\frac{\partial v^{(0)}}{\partial y}\right)dp\,\frac{\partial v^{(0)}}{\partial p}, \quad \text{and} \tag{2.23c}$$

$$\begin{aligned}N_3=&-\frac{\partial}{\partial\tau}\frac{\partial}{\partial p}\left(\frac{1}{\tilde{\tilde{\sigma}}}\frac{\partial\phi^{(0)}}{\partial p}\right)-\frac{\partial}{\partial p}\left[\frac{u^{(0)}}{\tilde{\tilde{\sigma}}}\frac{\partial}{\partial x}\frac{\partial\phi^{(0)}}{\partial p}+\frac{v^{(0)}}{\tilde{\tilde{\sigma}}}\frac{\partial}{\partial y}\frac{\partial\phi^{(0)}}{\partial p}\right]+\frac{1}{\tilde{\tilde{\sigma}}}\frac{\partial^2\phi^{(0)}}{\partial p^2}\left(\frac{\partial u^{(0)}}{\partial x}+\frac{\partial v^{(0)}}{\partial y}\right)\\&-\tilde{\tilde{\rho}}_T\frac{\partial\phi^{(0)}}{\partial t}\Bigg|_{p=\tilde{p}_T}\frac{1}{\tilde{\tilde{\sigma}}}\frac{\partial}{\partial p}\frac{\partial^2\phi^{(0)}}{\partial p^2}+\frac{1}{\tilde{\tilde{\sigma}}}\frac{\partial}{\partial p}\frac{\partial^2\phi^{(0)}}{\partial p^2}\int_{\tilde{p}_T}^{p}\left(\frac{\partial u^{(0)}}{\partial x}+\frac{\partial v^{(0)}}{\partial y}\right)dp+\frac{(1-\kappa)}{p\,\tilde{\tilde{\sigma}}}\frac{\partial\phi^{(0)}}{\partial p}\left(\frac{\partial u^{(0)}}{\partial x}+\frac{\partial v^{(0)}}{\partial y}\right)\\&+\tilde{\tilde{\rho}}_T\frac{\partial\phi^{(0)}}{\partial t}\Bigg|_{p=\tilde{p}_T}\frac{(1-\kappa)}{p^2\,\tilde{\tilde{\sigma}}}\frac{\partial\phi^{(0)}}{\partial p}-\frac{(1-\kappa)}{p^2\,\tilde{\tilde{\sigma}}}\frac{\partial\phi^{(0)}}{\partial p}\int_{\tilde{p}_T}^{p}\left(\frac{\partial u^{(0)}}{\partial x}+\frac{\partial v^{(0)}}{\partial y}\right)dp-\tilde{\tilde{\rho}}_T\frac{\partial\phi^{(0)}}{\partial t}\Bigg|_{p=\tilde{p}_T}\frac{(1-\kappa)}{p\,\tilde{\tilde{\sigma}}}\frac{\partial^2\phi^{(0)}}{\partial p^2}\\&+\frac{(1-\kappa)}{p\,\tilde{\tilde{\sigma}}}\frac{\partial^2\phi^{(0)}}{\partial p^2}\int_{\tilde{p}_T}^{p}\left(\frac{\partial u^{(0)}}{\partial x}+\frac{\partial v^{(0)}}{\partial y}\right)dp.\end{aligned} \tag{2.23d}$$

In (2.21)–(2.23), the mode amplitudes are held constant during the integration in t. The effect of this approach is to make $A_a(\varepsilon t)$ to vary in such a way as to eliminate the secular terms. In this way, the nonlinear products in (2.21)–(2.23) contain sums and differences of the time frequencies as arguments of the complex exponentials that define their time dependence. When the arguments are nonzero, the integrals will tend to zero, due to the fast fluctuations in t. On the other hand, when the arguments are zero (or nearly so, i.e., when $\varpi_a\approx\varpi_b+\varpi_c$) the integrals will tend to 1. Therefore, from (2.21)–(2.23) it follows straightforwardly that if one expresses $u^{(0)}$, $v^{(0)}$, and $\phi^{(0)}$ in terms of (2.10) truncated in such a way as to consider only a triad of modes a, b, and c satisfying the resonance conditions $\varpi_a\approx\varpi_b+\varpi_c$, $k_a=k_b+k_c$, and $n_a+n_b+n_c=$ odd, Eq. (2.21) can be written as

$$c_a^2\frac{dA_a}{d\tau}=A_bA_c\eta_a^{bc}, \tag{2.24a}$$

$$c_b^2\frac{dA_b}{d\tau}=A_aA_c^*\eta_b^{ac}, \quad \text{and} \tag{2.24b}$$

$$c_c^2\frac{dA_c}{d\tau}=A_aA_b^*\eta_c^{ab}. \tag{2.24c}$$

The nonlinear coupling coefficients η_a^{bc}, η_b^{ac}, and η_c^{ab} in (2.24) are given by

$$\eta_a^{bc} = -\langle \mathbf{B}\cdot\boldsymbol{\xi}_a(y)\rangle - \int_{-\infty}^{+\infty}\left\{\phi_a(y)\left[\phi_b i\varpi_c\phi_c\left(\frac{\tilde{\bar{\rho}}}{{c_b}^2}+\tilde{\bar{\Gamma}}\right)-\Lambda\,\tilde{\bar{\rho}}\phi_b\left(ik_c u_c+\frac{dv_c}{dy}\right)+\mathrm{CP}\right]\frac{G_a(p)G_b(p)G_c(p)}{\|G_a\|^2}\right\}\Bigg|_1^{\bar{p}_T} dy, \tag{2.25a}$$

with the inner product $\langle\cdot\rangle$ defined according to (2.17). The vector $\mathbf{B}$ in (2.25a) is defined by

$$\mathbf{B}=\begin{bmatrix}\left(u_b ik_c u_c+v_b\dfrac{du_c}{dy}\right)\alpha_a^{bc}+i\varpi_b\phi_b u_c\mu_a^{bc}-\left(ik_b u_b+\dfrac{dv_b}{dy}\right)u_c\theta_a^{bc}+\mathrm{CP}\\ \left(u_b ik_c v_c+v_b\dfrac{dv_c}{dy}\right)\alpha_a^{bc}+i\varpi_b\phi_b v_c\mu_a^{bc}-\left(ik_b u_b+\dfrac{dv_b}{dy}\right)v_c\theta_a^{bc}+\mathrm{CP}\\ \left(u_b ik_c\phi_c+v_b\dfrac{d\phi_c}{dy}\right)\vartheta_a^{bc}+i\varpi_b\phi_b\phi_c\Psi_a^{bc}-\left(ik_b u_b+\dfrac{dv_b}{dy}\right)\phi_c\varsigma_a^{bc}+\mathrm{CP}\end{bmatrix}, \tag{2.25b}$$

where α_a^{bc}, μ_a^{bc}, θ_a^{bc}, ϑ_a^{bc}, Ψ_a^{bc}, and ς_a^{bc} represent the interaction coefficients among the vertical eigenfunctions of modes a, b, and c and are expressed by

$$\alpha_a^{bc}=\frac{1}{\|G_a\|^2}\int_{\bar{p}_T}^1 G_b(p)G_c(p)G_a(p)\,dp,$$

$$\mu_a^{bc}=\frac{1}{\|G_a\|^2}\int_{\bar{p}_T}^1 \tilde{\bar{\rho}}_T G_b(\tilde{p}_T)\frac{dG_c}{dp}G_a(p)\,dp,$$

$$\theta_a^{bc}=\frac{1}{\|G_a\|^2}\int_{\bar{p}_T}^1 \frac{dG_c}{dp}\left(\int_{\bar{p}_T}^p G_b(p)\,dp\right)G_a(p)\,dp,$$

$$\vartheta_a^{bc}=\frac{1}{\|G_a\|^2}\int_{\bar{p}_T}^1 \left[G_b\frac{G_c}{{c_c}^2}-\frac{1}{\tilde{\bar{\sigma}}}\frac{dG_b}{dp}\frac{dG_c}{dp}\right]G_a(p)\,dp,$$

$$\Psi_a^{bc}=\frac{1}{\|G_a\|^2}\int_{\bar{p}_T}^1 \left[\frac{1}{{c_c}^2}\frac{dG_c}{dp}+\frac{(1-\kappa)}{p^2\tilde{\bar{\sigma}}}\frac{dG_c}{dp}+\frac{(1-\kappa)}{p}\frac{G_c}{{c_c}^2}\right]\tilde{\bar{\rho}}_T G_b(\tilde{p}_T)G_a(p)\,dp, \quad \text{and}$$

$$\varsigma_a^{bc}=\frac{1}{\|G_a\|^2}\int_{\bar{p}_T}^1 \left[\frac{G_c}{{c_c}^2}G_b+\frac{1}{{c_c}^2}\frac{dG_c}{dp}\int_{\bar{p}_T}^p G_b\,dp-\frac{(1-\kappa)}{p\tilde{\bar{\sigma}}}\frac{dG_c}{dp}G_b+\frac{(1-\kappa)}{p^2\tilde{\bar{\sigma}}}\frac{dG_c}{dp}\int_{\bar{p}_T}^p G_b\,dp+\frac{(1-\kappa)}{p}\frac{G_c}{{c_c}^2}\int_{\bar{p}_T}^p G_b\,dp\right]$$
$$G_a(p)\,dp. \tag{2.25c}$$

The terms CP in (2.25) indicate cyclical permutations between the superscripts b and c and $\|G_a\|$ corresponds to the norm of the vertical eigenfunctions. The condition $n_a + n_b + n_c =$ odd ensures that the resonant forcing has even symmetry about the equator. In case of an odd symmetry about the equator, the resonant component generated in the domain $y \geq 0$ would be exactly cancelled by the resonant component generated in the domain $y \leq 0$.

3. Energy relations

The total energy conservation principle for model equations (2.1)–(2.6) can be expressed as

$$\varepsilon^2\frac{\partial}{\partial t}\int_{-\tilde{L}_x}^{\tilde{L}_x}\int_{-\infty}^{+\infty}\left\{\int_{\bar{p}_T}^1\left[\frac{u^{(0)2}+v^{(0)2}}{2}+\frac{1}{2\tilde{\bar{\sigma}}}\left(\frac{\partial\phi^{(0)}}{\partial p}\right)^2\right]dp+\frac{\tilde{\bar{\rho}}\phi^{(0)2}}{2}\Bigg|_{\bar{p}_T}^1\right\}dy\;dx+O(\varepsilon^3)=0. \tag{3.1}$$

Thus, by inserting (2.10) into (3.1), integrating by parts the second term in (3.1) over p, and making use of (2.11a, b) and the orthogonality of the eigenmodes, we obtain Parseval's identity for the leading-order energy:

$$E^{(0)}=\sum_a c_a^2 A_a A_a^*=\sum_a c_a^2|A_a|^2. \tag{3.2}$$

Therefore, from the asymptotic reduced triad Eqs. (2.24), it follows that

TABLE 2. Vertical interaction coefficients α_m^{jl} evaluated from (2.25c) for $m = 0$, $m = 1$, and $m = 2$.

$m = 0$					
j^l	0	1	2	3	4
0	1.056 072 563	3.615×10^{-2}	-5.571×10^{-3}	3.815×10^{-3}	-1.376×10^{-3}
1	3.615×10^{-2}	1.047 619 589	2.907×10^{-2}	-5.421×10^{-3}	3.846×10^{-3}
2	-5.571×10^{-3}	2.907×10^{-2}	1.051 895 409	2.711×10^{-2}	-4.836×10^{-3}
3	3.815×10^{-3}	-5.421×10^{-3}	2.711×10^{-2}	1.052 738 106	2.655×10^{-2}
4	-1.376×10^{-3}	3.846×10^{-3}	-4.836×10^{-3}	2.655×10^{-2}	1.053 037 056
$m = 1$					
j^l	0	1	2	3	4
0	3.615×10^{-2}	1.047 619 589	2.907×10^{-2}	-5.421×10^{-3}	3.846×10^{-3}
1	1.047 619 589	-7.179×10^{-2}	0.744 051 375	1.883×10^{-2}	-5.045×10^{-3}
2	2.907×10^{-2}	0.744 051 375	-4.389×10^{-2}	0.744 540 491	1.541×10^{-2}
3	-5.421×10^{-3}	1.883×10^{-2}	0.744 540 491	-3.973×10^{-2}	0.744 663 554
4	3.846×10^{-3}	-5.045×10^{-3}	1.541×10^{-2}	0.744 663 554	-3.833×10^{-2}
$m = 2$					
j^l	0	1	2	3	4
0	-5.571×10^{-3}	2.907×10^{-2}	1.051 895 409	2.711×10^{-2}	-4.836×10^{-3}
1	2.907×10^{-2}	0.744 051 375	-4.389×10^{-2}	0.744 540 491	1.541×10^{-2}
2	1.051 895 409	-4.389×10^{-2}	1.336×10^{-2}	-2.027×10^{-2}	0.744 976 395
3	2.711×10^{-2}	0.744 540 491	-2.027×10^{-2}	9.227×10^{-3}	-1.619×10^{-2}
4	-4.836×10^{-3}	1.541×10^{-2}	0.744 976 395	-1.619×10^{-2}	8.057×10^{-3}

$$\frac{dE_a}{d\tau} = 2i\eta_a^{bc}\,\mathrm{Im}(A_a^* A_b A_c), \tag{3.3a}$$

$$\frac{dE_b}{d\tau} = 2i\eta_b^{ac}\,\mathrm{Im}(A_a A_b^* A_c^*), \quad \text{and} \tag{3.3b}$$

$$\frac{dE_c}{d\tau} = 2i\eta_c^{ab}\,\mathrm{Im}(A_a A_b^* A_c^*), \tag{3.3c}$$

where $E_j = c_j^2 |A_j|^2$ for $j = a$, b, and c represents the energy of the triad components. Thus, for the leading-order energy to be conserved in a resonant triad, the coupling coefficients must satisfy the relation

$$-\eta_a^{bc} + \eta_b^{ac} + \eta_c^{ab} = 0. \tag{3.4}$$

Equations (3.3) and (3.4) show that the wave having the coupling coefficient with the highest absolute value always gains energy from (or supplies energy to) the remaining triad components.

4. Determination of possible resonant triads

The goal of this section is to find triads of waves satisfying the kinematic resonance conditions $\varpi_a = \varpi_b + \varpi_c$, $k_a = k_b + k_c$, and $n_a + n_b + n_c = \text{odd}$. However, before seeking solutions of this algebraic system, it is important to know how the vertical structure of the waves restricts the interaction among them. According to (2.25), the coupling among the waves of a resonant triad through their vertical structures is measured by the coefficients α_a^{bc}, μ_a^{bc}, θ_a^{bc}, ϑ_a^{bc}, Ψ_a^{bc}, and ς_a^{bc}, as well as by the coupling terms at the boundaries given by the second term in the right-hand side of (2.25a). Table 2 displays the values of the interaction coefficient α_m^{jl} for the vertical eigenmodes $m = 0$, 1, and 2 and $0 \le j \ge 4$ and $0 \le l \ge 4$. This coefficient was evaluated from (2.25c) by using the trapezoidal rule. The calculations illustrated in Table 2 were performed for $\overline{\sigma} = 2 \times 10^{-6}$ $\mathrm{m^4\ s^2\ kg^{-2}}$, $L = 1.5 \times 10^6$ m, $\beta = 2.3 \times 10^{-11}$ $\mathrm{m^{-1}\ s^{-1}}$, $p_0 = 1000$ hPa, and $p_T = 150$ hPa. These values are fixed in all the calculations displayed hereafter in this paper. The interaction coefficient α_a^{bc} measures the coupling among the vertical structures of modes a, b, and c of a resonant triad through the horizontal advection of momentum. From Table 2 one notices that, in general, the trios whose vertical eigenmodes satisfy the relation $m = \pm j \pm l$ or similarly $\lambda_m \approx \pm\lambda_j \pm \lambda_l$ have the most significant interactions through the momentum horizontal advection. The other vertical interaction coefficients also demonstrate that these modes satisfying the relation $\lambda_m \approx \pm\lambda_j \pm \lambda_l$ for their vertical eigenvalues have in general the most significant coupling among their vertical structure eigenfunctions (tables not shown). Conversely, this resonance condition imposed by the vertical structure of the waves is no longer excluding, unlike the conditions imposed by the zonal wavenumbers and meridional modes. This selective rather than excluding nature of the resonance condition

imposed by the vertical structure of the waves can be clearly noted in Table 2, which shows that the interaction coefficient α_a^{bc} associated with trios whose vertical modes do not satisfy this condition is small but not zero.

The relation $\lambda_m \approx \pm\lambda_j \pm \lambda_l$ is an approximation of the familiar wavenumber summation rule that occurs when trigonometric functions describe the dependence. In this context, the reason for the small but not zero values of the interaction coefficient α_a^{bc} for trios whose vertical eigenvalues do not satisfy this condition is that, unlike the zonal wavenumbers, the vertical eigenvalues given by (2.12) are not exactly multiples of each other. Thus, this selective rather than excluding nature of the resonance condition imposed by the vertical structure of the waves is a consequence of the nature of the partial differential equations (2.1) and the boundary conditions (2.6), which determine the vertical eigenvalues λ_m and the vertical functional dependence of the linear eigenmodes. The effect of this nonexcluding nature of the resonance condition imposed by the vertical structure of the waves is to enable a larger number of triads to exist. This implies that the vertical stratification of the atmosphere spreads the possibility of triad interactions.

Nonetheless, in spite of the nonexcluding nature of the vertical resonance condition $\lambda_m \approx \pm\lambda_j \pm \lambda_l$, the wave triads whose vertical eigenvalues satisfy this relation have the most significant coupling among their vertical structure eigenfunctions and, consequently, undergo the most significant interactions. Therefore, we shall focus our analysis here on such resonant triads.

Regarding possible resonant triads among equatorial waves, it is important to mention that because of the nondispersive nature and the symmetric about the equator structure of the Kelvin waves, any triad of Kelvin wave components associated with the same vertical eigenmode does satisfy the resonance conditions $\varpi_a = \varpi_b + \varpi_c$, $k_a = k_b + k_c$, and $n_a + n_b + n_c =$ odd and, therefore, all the components of a Kelvin wave pack associated with the same vertical eigenmode are resonant with each other. In this sense, the barotropic Kelvin wave self-interactions are believed to be the most significant ones because they do satisfy the resonance condition in the vertical direction. On the other hand, the resonances involving the dispersive equatorial waves are sparse and, in general, nonlocal in the wavenumber space. Furthermore, due to the discrete spectrum of zonal wavenumbers that results from the periodic boundary condition in the x direction, the resonance condition for the time frequencies is not easily satisfied for dispersive waves, making its occurrence the exception instead of the rule. The resonant triads involving dispersive equatorial waves have been determined graphically by overlapping two dispersion curve plots in such a way that the origin of one plot is symmetrically displaced to a point on another dispersion curve. The produced intersection establishes a set of three normal modes satisfying the conditions $\varpi_a \approx \varpi_b + \varpi_c$ and $k_a = k_b + k_c$, provided that conditions $n_a + n_b + n_c =$ odd and $\lambda_a \approx \pm\lambda_b \pm \lambda_c$ are met. An exact resonance occurs when the two dispersion curve plots intersect exactly in one of the quantized zonal wavenumbers, which are indicated by the symbols marked along the dispersion curves of Fig. 3. Although this exact resonance is very difficult to be satisfied in practice, near resonances satisfy the relation $\varpi_a - \varpi_b - \varpi_c = O(\varepsilon)$, which is the actual condition for a significant interaction involving three quantized wavenumbers to take place at $O(\varepsilon)$ (Bretherton 1964).

Thus, examples of nearly resonant triads found by this graphical method involving dispersive equatorial waves are illustrated in Fig. 3 for triads composed of one barotropic Rossby wave and two first baroclinic equatorial waves. An interesting resonance is shown in Fig. 3a involving barotropic Rossby waves and first baroclinic mixed Rossby–gravity waves. Figure 3a shows a set of nearly resonant triads involving barotropic Rossby waves having the $n = 2$ meridional mode and mixed Rossby–gravity waves with the first baroclinic mode vertical structure, both having the same wavenumber $k > 2^{-1/2}$, coupled through a zonally symmetric geostrophic mode with the first baroclinic mode vertical structure and odd-meridional mode. It is interesting to note that all the Rossby and mixed Rossby–gravity waves with $k > 2^{-1/2}$ are nearly resonant with each other through any zonally symmetric geostrophic mode having an odd meridional mode. The most exact resonances refer to wavenumber 5 ($k \approx 1.175$) and the shortest waves (wavenumbers higher than 13 or $k > 3$). The triads associated with wavenumbers 4 ($k \approx 0.94$) and 5 are displayed in Table 3, which illustrates that the more equatorially trapped the geostrophic mode, the more expressive the interaction. Examples of the energy exchanges associated with these interactions will be shown in the next section.

Figure 3b shows a resonant triad composed of a zonal wavenumber-2 ($k \approx -0.47$) Kelvin wave, a $k = 0$ mixed Rossby–gravity mode, both with the $m = 1$ mode vertical structure, and a barotropic zonal wavenumber-2 ($k \approx 0.47$) Rossby wave with the second gravest meridional mode ($n = 2$). Figure 3c illustrates two nearly resonant triads composed of two first baroclinic mode westward inertio-gravity waves and a barotropic Rossby mode. In one of these triads, the inertio-gravity

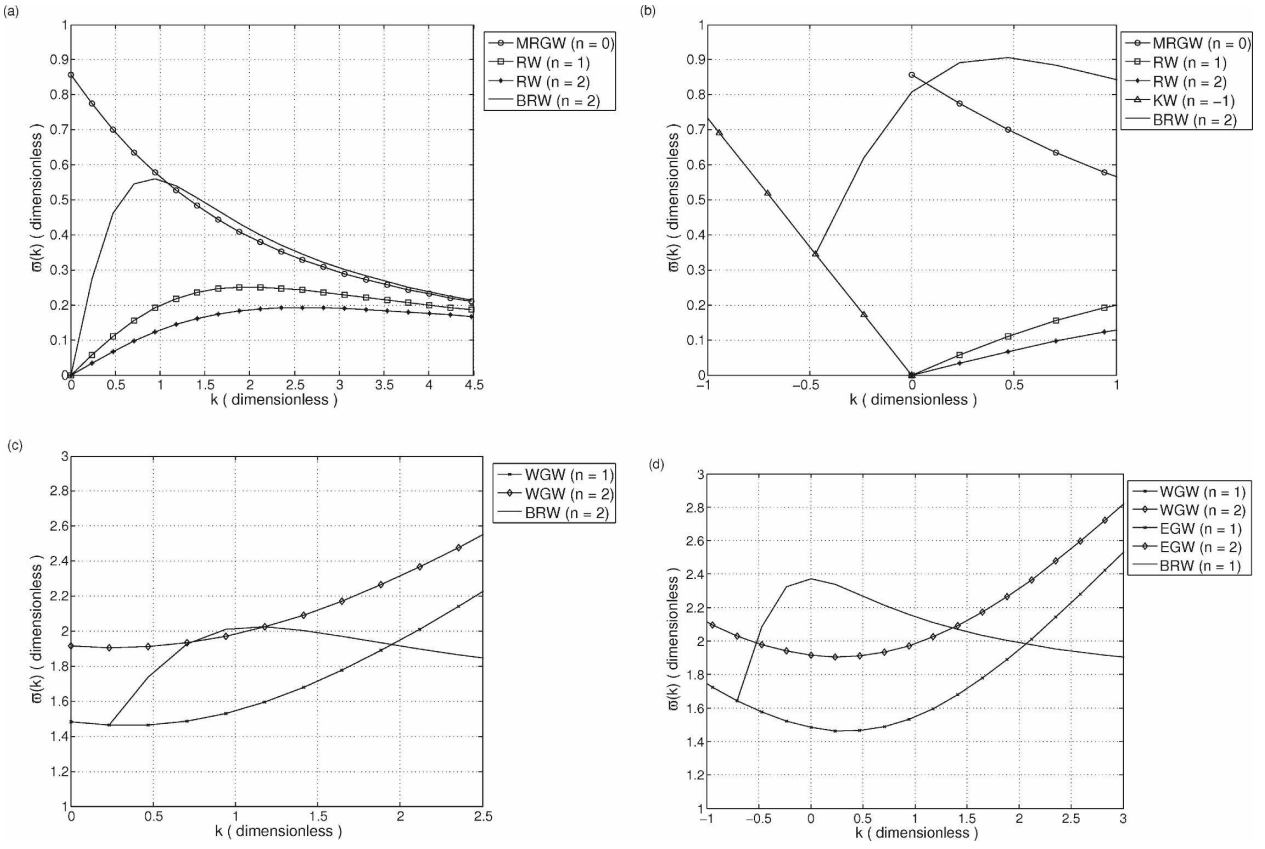

FIG. 3. Dispersion curves of the barotropic Rossby waves (BRWs) and the following first baroclinic mode equatorial waves: MRGWs, RWs, Kelvin waves (KWs), WGWs, and EGWs. Fig. 3a highlights the resonance involving BRWs and MRGWs through the zonally symmetric geostrophic mode with meridional mode $n = -1$ (Kelvin mode) and the $m = 1$ baroclinic mode vertical structure. Fig. 3b highlights the resonance involving a zonal wavenumber-2 KW, a $k = 0$ mixed Rossby–gravity mode and a zonal wavenumber-2 BRW with the second gravest meridional mode ($n = 2$). Fig. 3c highlights two resonances: one involving a WGW with zonal wavenumber 3 and meridional mode $n = 2$, a WGW with zonal wavenumber 1 and meridional mode $n = 1$, and a BRW with zonal wavenumber 2 and meridional mode $n = 2$; and the other involving a zonal wavenumber-5 WGW with meridional mode $n = 2$, a zonal wavenumber-1 WGW with meridional mode $n = 1$, and a zonal wavenumber-4 BRW with meridional mode $n = 2$. Fig. 3d indicates the resonance involving a zonal wavenumber-9 WGW, a zonal wavenumber-3 EGW, and a zonal wavenumber-12 BRW, all of them with meridional mode $n = 1$. The curve plots have been constructed by setting $\overline{\sigma} = 2 \times 10^{-6}$ m^4 s^2 kg^{-2}, $L = 1.5 \times 10^6$ m, $p_0 = 1000$ hPa, and $p_T = 150$ hPa. The symbols marked along the curves of the first baroclinic equatorial waves indicate the points where the zonal wavenumbers are defined.

TABLE 3. Numerical values of the resonant triads shown in Fig. 3. The table shows, from left to right, the triad components and their respective eigenfrequencies and coupling coefficients. The modes are characterized, from left to right, by the vertical eigenmode, the zonal wavenumber, the meridional mode, and the wave type: Rossby (R), Kelvin (K), mixed Rossby–gravity (M), westward inertio-gravity (WG), and eastward inertio-gravity (EG) waves. The calculations have been performed by setting $p_0 = 1000$ hPa, $p_T = 150$ hPa, $\overline{\sigma} = 2 \times 10^{-6}$ m^4 s^2 kg^{-2}, $L = 1500$ km, and $\beta = 2.3 \times 10^{-11}$ m^{-1} s^{-1}.

	a	b	c	ϖ_a	ϖ_b	ϖ_c	$i\eta_a^{bc}$	$i\eta_b^{ac}$	$i\eta_c^{ab}$
1	0, 4, 2, R	1, 4, 0, M	1, 0, −1, K	0.56	0.58	0	0.228	0.324	0.00
2	0, 4, 2, R	1, 4, 0, M	1, 0, 1, R	0.56	0.58	0	0.061	0.106	0.00
3	0, 5, 2, R	1, 5, 0, M	1, 0, −1, K	0.54	0.527	0	0.425	0.524	0.00
4	0, 5, 2, R	1, 5, 0, M	1, 0, 1, R	0.54	0.527	0	0.242	0.287	0.00
5	1, 0, 0, M	0, 2, 2, R	1, −2, −1, K	0.856	0.462	0.345	0.2	0.119	0.045
6	1, 3, 2, WG	1, 1, 1, WG	0, 2, 2, R	1.93	1.46	0.46	0.095	0.07	0.0186
7	1, 5, 2, WG	1, 1, 1, WG	0, 4, 2, R	2.02	1.46	0.56	0.296	0.215	0.064
8	1, 9, 1, WG	1, 3, 1, EG	0, 12, 1, R	2.01	1.64	0.33	0.727	0.623	0.0814

waves have zonal wavenumbers 1 ($k \approx 0.235$) and 3 ($k \approx 0.705$) and meridional modes $n = 1$ and $n = 2$, respectively, whereas the Rossby mode is characterized by a zonal wavenumber 2 ($k \approx 0.47$) and meridional mode $n = 2$; on the other triad, the inertio-gravity waves have zonal wavenumbers 1 and 5 and meridional modes $n = 1$ and $n = 2$, respectively, whereas the barotropic Rossby wave is characterized by a zonal wavenumber 4 and meridional mode $n = 2$. A resonant triad composed of a zonal wavenumber-3 eastward inertio-gravity wave, a zonal wavenumber-9 westward inertio-gravity wave (both with the $n = 1$ meridional mode and the first baroclinic mode vertical structure), and a barotropic Rossby wave with zonal wavenumber 12 and meridional mode $n = 1$ is shown in Fig. 3d. The other resonance found in Fig. 3d involving an $n = 2$ westward inertio-gravity wave does not satisfy the condition $n_a + n_b + n_c = \text{odd}$.

The resonant triads displayed in Fig. 3 are summarized in Table 3. Table 3 displays the triad components and their respective eigenfrequencies and coupling coefficients. The coupling coefficients η_a^{bc}, η_b^{ac}, and η_c^{ab} were evaluated from (2.25a) by using the Gauss–Hermite quadrature formula. Table 3 shows that, in general, the coupling coefficients are proportional to the individual eigenfrequencies in the resonant triads. Consequently, in the atmospheric model adopted here the highest absolute frequency mode in a resonant triad is in general the most energetically active member of the triad, that is, the triad component whose energy always grows (or decays) at the expense of the remaining triad components. This is a consequence of the conservation of the leading-order energy in the resonant interactions, as shown in section 3. This energetic property of the resonant triads has also been found in the shallow-water equations (as discussed in section 1) as well as in several other problems in fluid mechanics, such as in the theory of surface–gravity waves in deep water and capillary–gravity waves. A complete review of the phenomenon of the three-wave resonance in fluid mechanics can be found in chapter 5 of Craik (1985). Another interesting consequence of this energetic property of the resonant triads is that the coupling coefficients of the zonally symmetric geostrophic modes are always zero in a resonant triad interaction involving two propagating modes, as illustrated in Table 3. As a consequence, these modes always work as catalyst components in a resonant interaction involving two propagating waves, allowing the waves with the same zonal wavenumber and nearly equal or opposite time frequencies to exchange energy without being affected by the propagating waves, as will be shown in the next section.

5. Dynamics of the resonant interactions

In this section, examples of the solution of the asymptotic reduced Eqs. (2.24) are shown for selected resonant triads to illustrate some aspects of the dynamics of the resonant interactions among equatorial waves in the present model. Because the nonlinear coupling coefficients η_a^{bc}, η_b^{ac}, and η_c^{ab} are purely imaginary, analytical solutions for system (2.24) are obtainable. Considering the mode having the coupling coefficient with the highest absolute value as mode a and the mode having the smallest absolute coupling coefficient as mode c, it follows that—subject to the initial condition $|A_a(t = 0)| = 0$, $|A_b(t = 0)| = R_b^0$, and $|A_c(t = 0)| = R_c^0$—the solution of (2.24) is expressed in terms of the modes' energy as (see McGoldrick 1965 and Domaracki and Loesch 1977)

$$E_a(t) = c_a^2 (R_b^0)^2 \left(\left| \frac{\eta_a^{bc}}{\eta_b^{ac}} \right| \frac{c_b^2}{c_a^2} \right) \mathrm{sn}^2 \left(\frac{\Xi}{\tilde{m}} \right), \tag{5.1a}$$

$$E_b(t) = c_b^2 (R_b^0)^2 \mathrm{cn}^2 \left(\frac{\Xi}{\tilde{m}} \right), \quad \text{and} \tag{5.1b}$$

$$E_c(t) = c_c^2 (R_c^0)^2 \mathrm{dn}^2 \left(\frac{\Xi}{\tilde{m}} \right), \tag{5.1c}$$

where sn, cn, and dn are the Jacobian elliptic functions (Abramowitz and Stegun 1964, chapter 16), having the argument

$$\Xi = R_c^0 \left(\frac{|\eta_a^{bc} \eta_b^{ac}|}{c_a^2 c_b^2} \right)^{(1/2)} \varepsilon t$$

and parameter

$$\tilde{m} = \frac{\eta_c^{ab}}{\eta_b^{ac}} \frac{c_b^2}{c_c^2} \frac{(R_b^0)^2}{(R_c^0)^2}.$$

Because the frequency of the energy (amplitude) modulation is proportional to R_c^0 and the parameter $\tilde{m}$ is dependent in part upon the ratio R_b^0/R_c^0, the period of the energy exchanges can be arbitrarily long or short depending on the initial wave amplitudes. If $\tilde{m} = 0$ ($\eta_c^{ab} = 0$), the solution (5.1) becomes

$$E_a(t) = c_a^2 (R_b^0)^2 \left(\left| \frac{\eta_a^{bc}}{\eta_b^{ac}} \right| \frac{c_b^2}{c_a^2} \right) \sin^2 \left(\frac{\Xi}{\tilde{m}} \right), \tag{5.2a}$$

$$E_b(t) = c_b^2 (R_b^0)^2 \cos^2 \left(\frac{\Xi}{\tilde{m}} \right), \quad \text{and} \tag{5.2b}$$

$$E_c(t) = E_c(t = 0) = \text{constant}. \tag{5.2c}$$

In this case, the energy of mode c remains constant. Its role is to act as a catalyst for the energy exchange between modes a and b, in the sense that it enables the

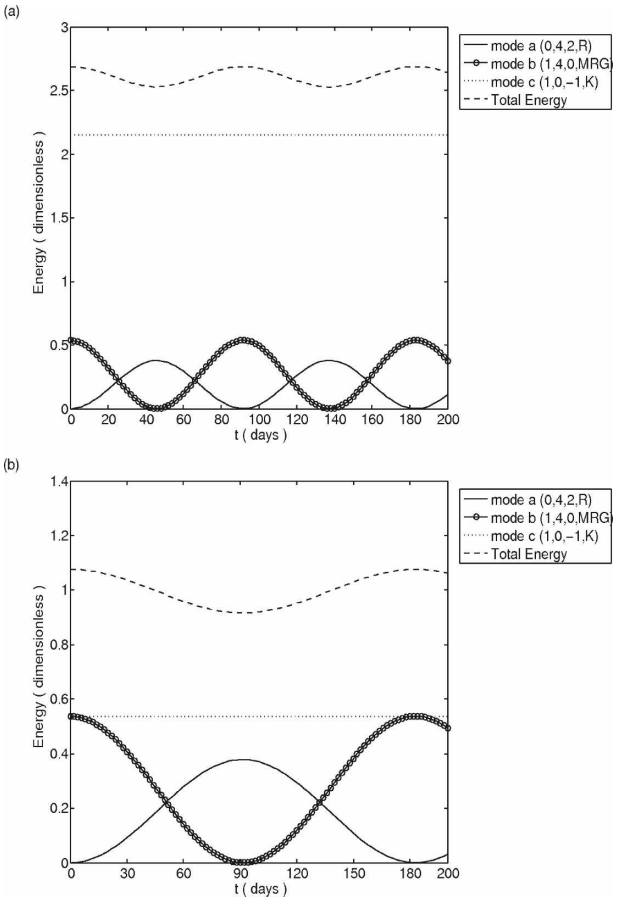

FIG. 4. Time evolution of the mode energies for the triad composed of a barotropic Rossby wave with zonal wavenumber 4 ($k \approx 0.94$) and meridional mode $n = 2$ (mode a), a mixed Rossby–gravity wave with zonal wavenumber 4 ($k \approx 0.94$) and vertical mode $m = 1$ (mode b), and a zonally symmetric Kelvin mode ($n = -1$) having the vertical mode $m = 1$ (mode c). The initial amplitudes are set as (a) $R_b^0 = 1$ and $R_c^0 = 2$ and (b) $R_b^0 = R_c^0 = 1$.

resonance conditions to be satisfied and controls the interaction period via its initial amplitude R_c^0. This is exactly the case of the triads involving first baroclinic mixed Rossby–gravity and barotropic Rossby waves with the same wavenumber and the zonally symmetric geostrophic modes with odd meridional mode found in section 4. Figure 4 illustrates the energy exchanges for triad 1 of Table 3, which is composed of a barotropic Rossby wave with zonal wavenumber 4 ($k \approx 0.94$) and meridional mode $n = 2$ (mode a), a mixed Rossby–gravity wave with zonal wavenumber 4 and the first baroclinic mode vertical structure (mode b) and a zonally symmetric ($k = 0$) Kelvin mode ($n = -1$) with the same vertical structure as the mixed Rossby–gravity wave (mode c). Figure 4a shows the time evolution of the mode energies for the initial amplitudes given by $R_b^0 = 1$ and $R_c^0 = 2$, whereas Fig. 4b shows the same time evolution but for the initial amplitudes $R_b^0 = 1$ and $R_c^0 = 1$. In Fig. 4 and all other integrations shown in this section, we have set $U = 5\ \mathrm{m\,s^{-1}}$, $L = 1500$ km, and $\beta = 2.3 \times 10^{-11}\ \mathrm{m^{-1}\,s^{-1}}$, implying $\varepsilon = 0.097$. The role of the geostrophic mode in controlling the period of the energy exchange between the internal mixed Rossby–gravity mode and the barotropic Rossby wave is clearly noticeable by comparing Figs. 4a and 4b. As observed in Fig. 4, the mixed Rossby–gravity and Rossby modes exchange energy periodically, whereas the total energy is almost conserved. The small-amplitude oscillations in total energy observed in Fig. 4 are believed to be due to the small frequency mismatch among the triad modes because the coupling coefficients only satisfy the relation (3.4) for exact resonances. Thus, the leading-order energy given by (3.2) is only conserved for the resonant triads; that is, for the off-resonant triads, the higher-order terms of $O(\varepsilon^3)$ in (3.1) must be taken into account.

To analyze the implications of the energy exchanges observed in Fig. 4 for the solution in physical space, Figs. 5–7 illustrate some aspects of the physical space solution referred to the interaction shown in Fig. 4a. The quantities displayed in Figs. 5–7 are obtained by (2.10) truncated in such a way as to consider only the triad components of Fig. 4. Figure 5 displays the y–p cross section of the meridional wind (v) along the longitude of 22.5°W at (a) $t = 0$, (b) $t = 26$, (c) $t = 47$, and (d) $t = 67$ days. Because the meridional wind is zero for the zonally symmetric geostrophic modes (and also for the Kelvin modes), it is a useful quantity to observe the physical space manifestation of the energy exchanges between the Rossby and mixed Rossby–gravity waves shown in Fig. 4. At $t = 0$ the Rossby wave energy is zero and the meridional wind pattern observed in Fig. 5a is due to the internal mixed Rossby–gravity wave (mode b) activity. At this stage, the flow is essentially trapped in the equatorial region. At $t = 26$ days, the Rossby and mixed Rossby–gravity modes have the same energy level (Fig. 4a). As a result, the meridional wind pattern shown in Fig. 5b is due to both Rossby and mixed Rossby–gravity wave activity. The Rossby wave activity is clear in Fig. 5b from the centers of action near the latitudes of $\pm 60°$ with an essentially barotropic structure. In tropical latitudes, the superposition of the first baroclinic mixed Rossby–gravity wave and the barotropic Rossby wave yields a meridional wind pattern trapped in the upper troposphere. Conversely, at $t = 67$ days (Fig. 5d), the superposition of these modes leads to a tropical pattern essentially trapped in the lower troposphere. At $t = 47$ days, the meridional wind pattern shown in Fig. 5c is entirely due to the barotropic

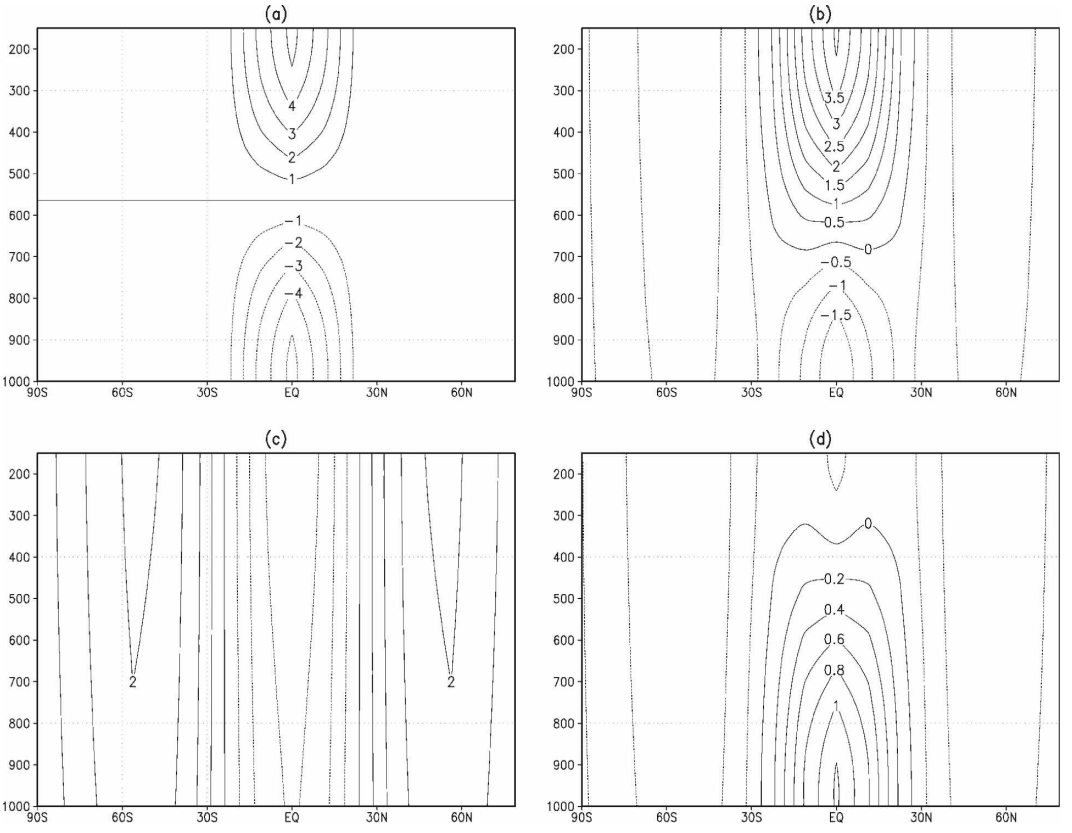

FIG. 5. Latitude vs pressure (hPa) cross section of the meridional wind along longitude of 22.5°W referred to the solution of Fig. 4a at (a) $t = 0$, (b) $t = 26$; (c) $t = 47$, and (d) $t = 67$ days. The meridional wind displayed in this figure has been obtained from expansion (2.10) truncated to consider only the modes of triad 1 of Table 3. The v field is shown in m s^{-1} using the scales in (2.3) for $U = 5$ m s^{-1}.

Rossby wave. It is noticeable that this mode is much less equatorially trapped than the first baroclinic mixed Rossby–gravity wave, having large amplitude in middle and high latitudes.

In fact, the meridional structure functions $\xi_a(y)$ associated with the barotropic mode are much less equatorially trapped than those associated with the baroclinic modes because the separation constant c_a appears as an e-folding length in the exponentially decaying part of the eigenfunction $\xi_a(y)$. As a consequence, the smaller the value of c_a, the more equatorially trapped the y structure of the eigenmode. In fact, the equatorial β plane is well known to be a good approximation for the internal modes of small equivalent depth (Lindzen 1967). For the barotropic mode, the equatorial β-plane approximation is not valid except for low meridional mode n; therefore a more accurate geometry and Coriolis term in (2.1) are necessary. Strictly speaking, the equatorial β-plane approximation is a valid one when the turning latitude y_T of the mode, which represents the distance from the equator where its y-structure function $\xi_a(y)$ changes from an oscillatory to an exponentially decaying behavior, is such that $|y_T| < |y_p|$ (Lindzen 1967; Silva Dias and Schubert 1979), where y_P refers to latitude of the pole. Using the values of c_m of Table 1, it follows that the turning latitude y_T for the barotropic mode corresponds to 58° and 75° for the meridional modes $n = 1$ and $n = 2$, respectively. Thus, all the barotropic Rossby waves of the resonant triads displayed in Table 3 are within the limit of validity of the equatorial β-plane approximation. For the first baroclinic mode, the validity condition is satisfied up to $n = 25$. The high amplitude of the barotropic Rossby modes in middle and high latitudes suggests that resonant interactions involving a barotropic Rossby mode and two internal equatorial waves might play an important role in tropics–midlatitude connection. The potential future extension of the wave interaction theory developed here for the real atmosphere will be discussed in section 6.

Figure 6 displays the horizontal distribution of the horizontal wind and geopotential fields at $p = 1000$ hPa associated with the solution of Fig. 4a at $t = 0$ (Fig. 6a) and at $t = 47$ days (Fig. 6b). The spatial structure of the

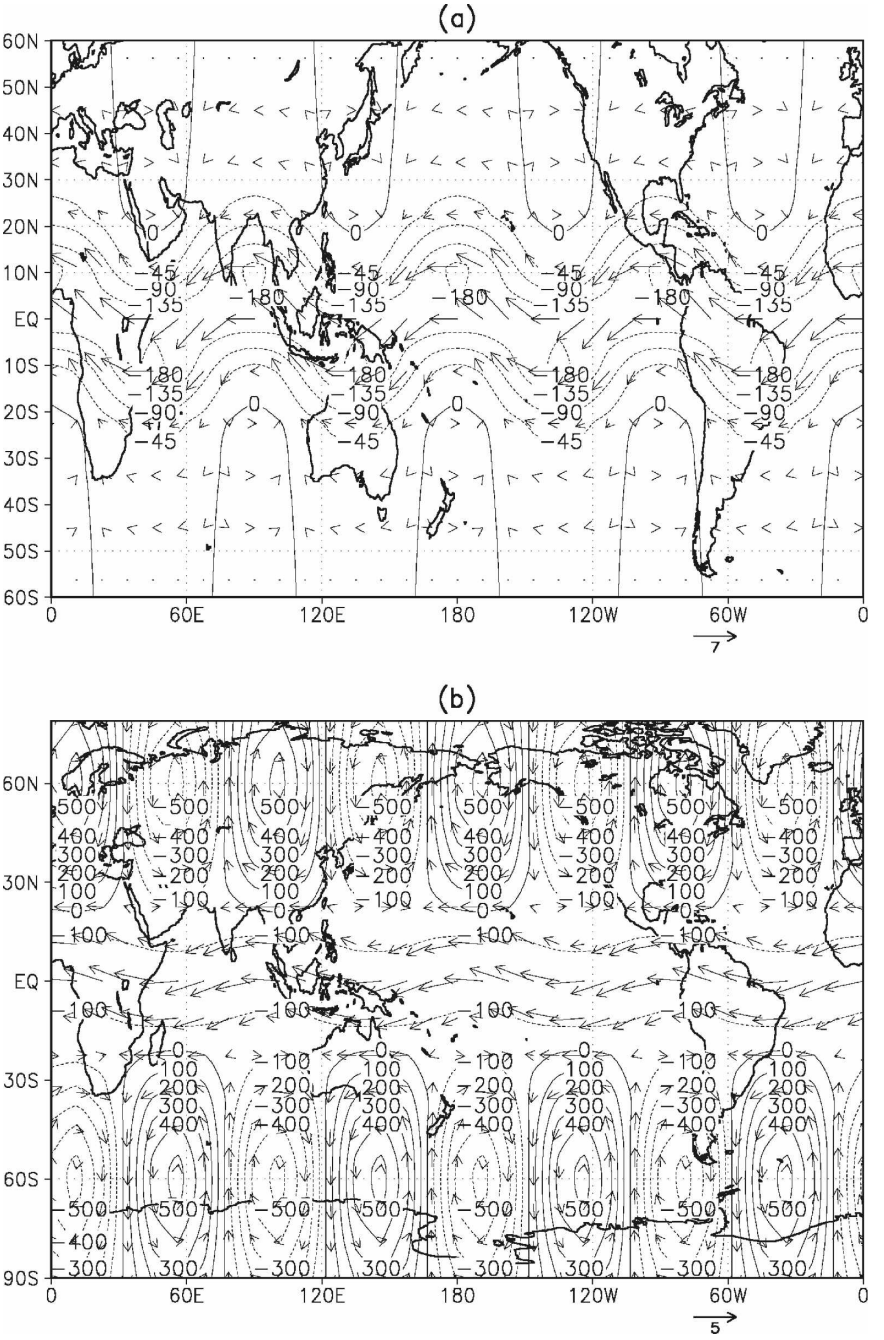

FIG. 6. Horizontal wind (vector) and geopotential (contour) fields at $p = 1000$ hPa associated with the same solution of Figs. 4a and 5 at (a) $t = 0$ and (b) $t = 47$ days. The horizontal wind and geopotential fields are shown in m s^{-1} and m^2 s^{-2}, respectively, using the scales in (2.3) for $U = 5$ m s^{-1}, $\beta = 2.3 \times 10^{-11}$ m^{-1} s^{-1}, and $L = 1.5 \times 10^6$m.

$k = 0$ Kelvin mode (mode c) can be clearly observed in Figs. 6a and 6b by the noticeable zonally symmetric easterly wind component and the zonally symmetric trough along the equatorial region. The small perturbations in this zonally homogeneous structure along the equator observed in Figs. 6a and 6b are due to the activity of the mixed Rossby–gravity wave and the barotropic Rossby mode, respectively. Figure 7 shows the time evolution of the 200-hPa horizontal divergence at 12.5°S, 22.5°W (Fig. 7a) and the 550-hPa meridional wind at 60°S, 22.5°W (Fig. 7b). Because the horizontal divergence is zero for the zonally symmetric geo-

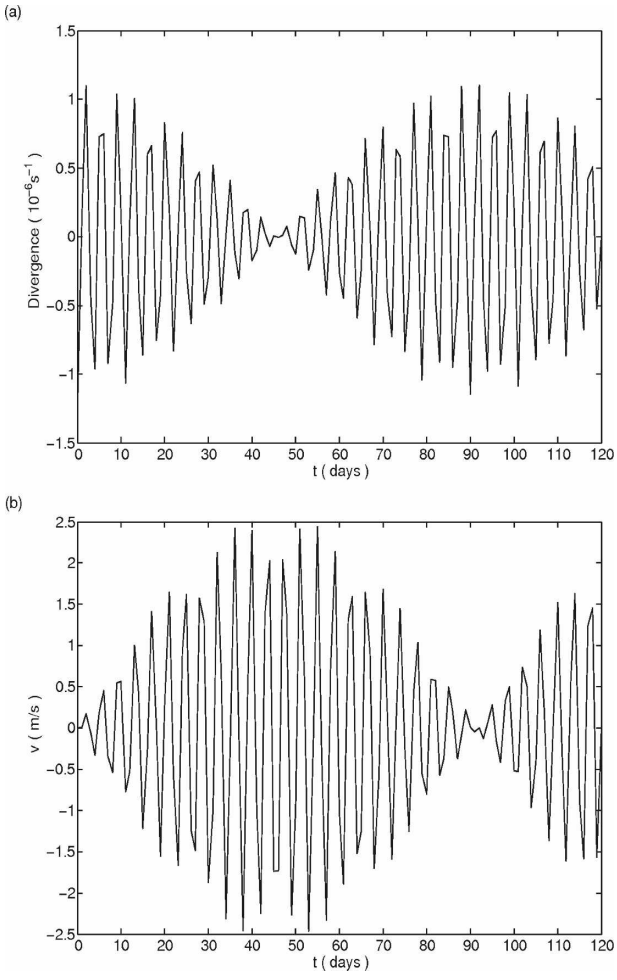

FIG. 7. Time evolution of the (a) 200-hPa horizontal divergence at 12.5°S, 22.5°W and (b) 550-hPa meridional wind at 60°S, 22.5°W associated with the solution of Figs. 4a, 5, and 6. The wind and the divergence are displayed in this figure in m s^{-1} and 10^{-6} s^{-1}, respectively, using the scales in (2.3) for $U = 5$ m s^{-1}, $\beta = 2.3 \times 10^{-11}$ m^{-1} s^{-1}, and $L = 1.5 \times 10^{6}$ m.

strophic modes and small for the barotropic Rossby waves, it essentially represents the baroclinic mixed Rossby–gravity wave activity in Fig. 7a. Similarly, once the waves associated with the internal modes have neglectable amplitude at $\pm 60°$ and the eigenfunction $G_1(p)$ is almost zero at $p = 550$ hPa (Fig. 2b), the time evolution of the 550-hPa meridional wind shown in Fig. 7b illustrates the activity of the barotropic Rossby wave of triad 1 of Table 3. The time evolution of the 200-hPa divergence and the 550-hPa meridional wind exhibits local oscillations with a period of the order of 4 days. These local oscillations are due to the phase propagation of the waves because both the Rossby and the mixed Rossby–gravity modes of triad 1 of Table 3 have a period of approximately 4 days. Apart from these high-frequency local oscillations, a longer time scale modulation in the amplitude of these local oscillations is also observed. Comparing Fig. 7 and Fig. 4a reveals that this longer time scale modulation is due to the energy exchanges between the Rossby and mixed Rossby–gravity waves displayed in Fig. 4a. In fact, the times when the magnitude of the divergence is maximal correspond exactly to the times when the energy of the baroclinic mixed Rossby–gravity wave peaks. On the other hand, when the energy of the barotropic Rossby wave is maximal (and the energy of the mixed Rossby–gravity wave is minimal), the amplitude of the divergence oscillations is minimal and the amplitude of the 550-hPa meridional wind is maximal.

Thus, Figs. 4–7 demonstrate that the periodic exchanges of energy among waves constituting a resonant triad imply periodic changes of regime in the physical space solution. Such changes of regime, in turn, occur in a longer time scale than the period of the local oscillations resulting from the phase propagation of the waves. This periodic change of regime in the solution in physical space due to the internal dynamics of the model is known as vacillation (Lorenz 1963). As observed in Figs. 5–7, the initial amplitudes set in Fig. 4 are realistic in the sense that they reproduce the typical magnitude of weather and climate anomalies. Consequently, with the initial amplitudes characterizing typical magnitudes of atmospheric flow perturbations, Fig. 4 shows that the mixed Rossby–gravity and Rossby modes of triad 1 of Table 3 exchange energy on intraseasonal or semiannual time scales, with the period of the energy exchange depending on the initial amplitude of the geostrophic mode.

The energy exchanges between the first baroclinic mixed Rossby–gravity wave and the barotropic Rossby wave with zonal wavenumber 5 ($k \approx 1.175$), composing triad 3 of Table 3, are illustrated in Fig. 8 for $R_b^0 = 1$ and $R_c^0 = 2$. Because the interaction in triad 3 is stronger than in triad 1, for the same initial energy distribution as in Fig. 4a, the interaction period for the internal mixed Rossby–gravity and barotropic Rossby waves with wavenumber 5 is of the order of 50 days. Another example of energy exchanges due to resonant triad interaction in the present model is illustrated in Fig. 9, which shows the time evolution of the mode energies associated with triad 5 of Table 3. This triad is composed of a $k = 0$ mixed Rossby–gravity mode (mode *a*), a zonal wavenumber-2 Kelvin wave (mode **c**) (both with the $m = 1$ mode vertical structure), and a zonal wavenumber-2 barotropic Rossby wave with $n = 2$ meridional mode (mode *b*). The initial amplitudes are set as $R_b^0 = 0.1$ and $R_c^0 = 2.0$ (Fig. 9a), $R_b^0 = 0.15$ and $R_c^0 = 1.2$ (Fig. 9b), and $R_b^0 = 0.192$ and $R_c^0 = 1.0$ (Fig. 9c). As

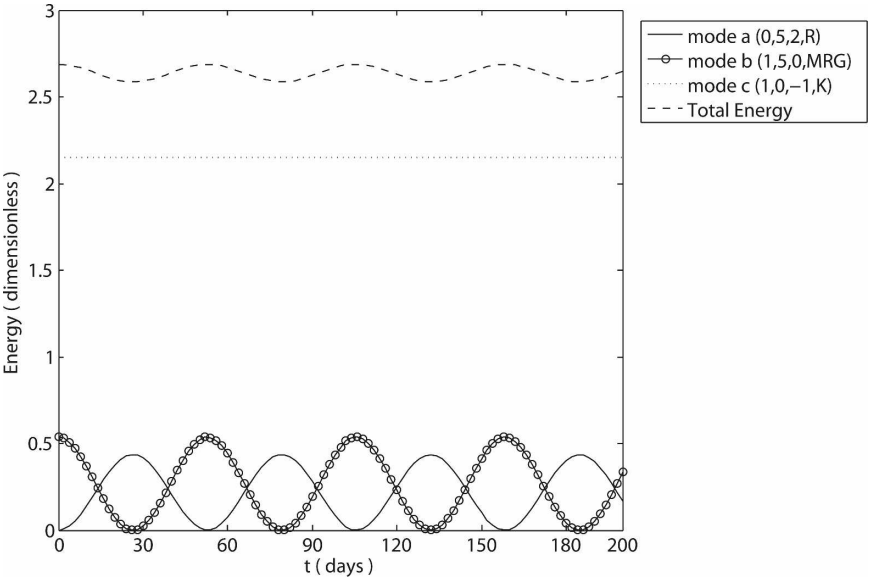

FIG. 8. As in Fig. 4a, but for the triad composed of a barotropic Rossby wave with zonal wavenumber 5 ($k \approx 1.175$) and meridional mode $n = 2$ (mode *a*), a mixed Rossby–gravity wave with zonal wavenumber 5 ($k \approx 1.175$) and vertical mode $m = 1$ (mode *b*), and a zonally symmetric Kelvin mode ($n = -1$) having the vertical mode $m = 1$ (mode *c*).

expected from the values of the coupling coefficients (Table 3), Fig. 9 shows that, in this resonant interaction, the mixed Rossby–gravity mode is the most energetically active member of the triad; that is, its energy always grows (or decays) at the expense of the Kelvin and Rossby modes. The Kelvin wave in this interaction is the less energetically active member.

The energy modulations of these modes can exhibit

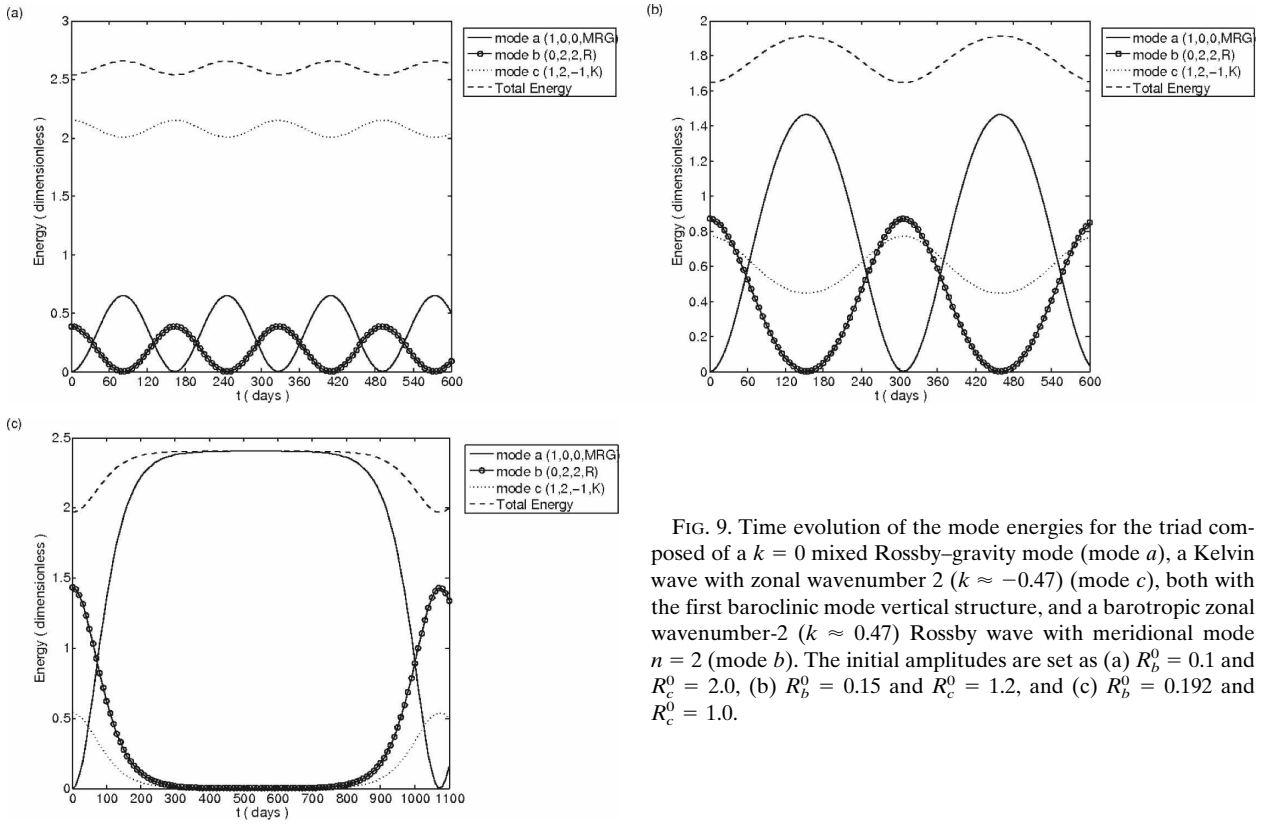

FIG. 9. Time evolution of the mode energies for the triad composed of a $k = 0$ mixed Rossby–gravity mode (mode *a*), a Kelvin wave with zonal wavenumber 2 ($k \approx -0.47$) (mode *c*), both with the first baroclinic mode vertical structure, and a barotropic zonal wavenumber-2 ($k \approx 0.47$) Rossby wave with meridional mode $n = 2$ (mode *b*). The initial amplitudes are set as (a) $R_b^0 = 0.1$ and $R_c^0 = 2.0$, (b) $R_b^0 = 0.15$ and $R_c^0 = 1.2$, and (c) $R_b^0 = 0.192$ and $R_c^0 = 1.0$.

different behaviors depending on the initial amplitudes of modes b and c because these initial amplitudes appear in the expression of the argument Ξ and the parameter $\tilde{m}$ of the Jacobian elliptic functions in the solution (5.1). Figure 9a shows a representative example of energy exchanges due to triad interaction when the parameter $\tilde{m}$ of the Jacobian elliptic functions is within the range $0 < \tilde{m} \ll 1$. In this case, the Kelvin mode of triad 5 of Table 3 essentially exhibits a similar behavior to the zonally symmetric geostrophic mode of the triads displayed in Figs. 4 and 8, acting as a catalyst for the energy exchanges between the barotropic Rossby and first baroclinic mixed Rossby–gravity modes. A qualitatively representative example of triad modulations when $0 < \tilde{m} < 1$ is shown in Fig. 9b. In this case, all the three modes undergo significant energy modulations. Figure 9c illustrates an interesting example of energy modulations in a resonant triad that occurs when $0 \ll \tilde{m} < 1$. The remarkable feature of the solution (5.1) in this situation is the extended time interval through which the energy of the $k = 0$ first baroclinic mixed Rossby–gravity mode is large and nearly constant. The other interesting feature of the energy solution displayed in Fig. 9c is the relatively rapid growth and decay phases of the energy of the modes. As can be observed in Fig. 9c, these rapid growth and decay stages of the modes' energy occupy only a small fraction of the total interaction period. As in Figs. 4 and 8, the small-amplitude modulation of total energy observed in Fig. 9 is due to the small frequency mismatch among the modes of triad 5 of Table 3.

Another important point to be highlighted here is that, as in Figs. 4–7, the initial amplitudes set in the simulations shown in Fig. 9 reproduce typical magnitudes of atmospheric flow disturbances (figures not shown). Thus, for the initial amplitudes characterizing realistic magnitudes of the wind and geopotential fields, the energy exchanges associated with this triad interaction can be arbitrarily long or short; that is, they can occur from semiannual to interannual time scales, depending on the initial wave amplitudes.

6. Remarks

A new attempt to describe the weakly nonlinear interaction of equatorial waves has been presented in this paper by using the adiabatic version of the equatorial β-plane primitive equations in isobaric coordinates. Assuming rigid lid vertical boundary conditions, the conditions imposed at the surface and at the top of the troposphere were expanded in a Taylor series around two isobaric surfaces in an approach similar to that used in the theory of surface–gravity waves in deep water and capillary–gravity waves. By adopting the asymptotic method of multiple time scales, the equatorial Rossby, mixed Rossby–gravity, inertio-gravity and Kelvin waves, as well as their vertical structures, were obtained as leading-order solutions. These waves were shown to be capable of resonant interactions at the $O(\varepsilon)$ approximation, enabling energy to be efficiently exchanged within a triad. The resonant triads whose wave components satisfy the relation $\lambda_m \approx \pm\lambda_j \pm \lambda_l$ for their vertical eigenvalues were found to have the most significant interactions, although this condition is not excluding, unlike the resonance conditions for the zonal wavenumbers and meridional modes. The effect of this nonexcluding nature of the resonance condition imposed by the vertical structure of the waves is to enable a larger number of triads to exist, implying that the vertical stratification of the atmosphere spreads the possibility of triad interactions. The results show that for these resonant triads satisfying the resonance condition in the vertical direction, the wave having the highest absolute frequency acts in general as an energy source (or sink) for the remaining triad components, as usually occurs in several other physical problems in fluid dynamics. In addition, the zonally symmetric geostrophic modes act as catalyst modes for the energy exchanges between two dispersive waves in a resonant triad. The integration of the reduced asymptotic equations for selected resonant triads shows that, for the initial mode amplitudes characterizing realistic magnitudes of atmospheric flow perturbations, the modes in general exchange energy on low-frequency (intraseasonal and/or even longer) time scales, with the interaction period being dependent upon the initial mode amplitudes.

Nevertheless, although these selected resonant triads undergo the most significant interactions, an important question that cannot be addressed in the context of our reduced dynamics of a single wave triad concerns the stability and/or robustness of these triad interactions. In fact, the periodic variations due to the triad interactions explored in this paper may be unstable with perturbations that have been excluded in our analysis. Nonlinear time integrations with the full system from the corresponding initial conditions are necessary to check the stability and the robustness of these resonances. In particular, the energy exchanges due to the triad interaction shown in Fig. 9 (triad 5 of Table 3) may be unstable with regard to the Kelvin mode self-interactions, even though these resonant harmonics are associated with the same internal vertical mode. Because of the nonexcluding nature of the resonance condition imposed by the vertical structure of the waves, all the components of the first baroclinic Kelvin mode are resonant with

each other. Consequently, the initial energy of the zonal wavenumber-2 Kelvin mode of triad 5 of Table 3 can leak to its harmonics and therefore weaken the energy exchanges observed in Fig. 9. We intend to address this issue regarding the robustness of the resonances studied here in a future paper.

Because of the high amplitude of the barotropic Rossby modes in middle and high latitudes, if we apply the wave interaction theory developed here to the real atmosphere, resonant triads like those shown in Table 3 composed of two first baroclinic equatorial waves and one barotropic Rossby mode might play an important role in the tropics–extratropics interaction on low-frequency time scales. In fact, the first baroclinic mode corresponds to the vertical mode most excited by the typical tropical heating associated with deep convection and dominates the energetics of the large-scale motions in the tropics (Silva Dias and Bonatti 1985). On the other hand, a significant portion of the energy of the atmospheric circulation is in equivalent barotropic modes, which are responsible for the propagation of energy from tropics to middle and high latitudes (Hoskins and Karoly 1981; Kasahara and Silva Dias 1986). Thus, energy exchanges due to resonant triad interactions involving equatorially trapped first baroclinic equatorial waves and barotropic Rossby modes with significant midlatitude projection can be potentially important for the global teleconnection patterns from tropics to midlatitudes as well as for the midlatitude influence on the tropical wave dynamics.

However, the application of the present theory to the real atmosphere requires the inclusion in the present model of some important physical processes in the atmosphere that have not been considered in the present analysis. These physical mechanisms include diabatic effects, boundary layer drag, and a more realistic $O(1)$ background flow in the governing equations (2.1)–(2.6). In fact, only seldom are the large-scale atmospheric disturbances perturbations from motionless basic states. Thus, the inclusion of a geostrophic basic state with both vertical and meridional shear and the analysis of its influence on the resonant triads obtained in this work should be studied, as well as the analysis of the influence of diabatic heating on these resonances. Moreover, diabatic heating can also resonantly couple the equatorial waves obtained here as leading-order solutions. Because the diabatic heating associated with deep convection in the tropics mostly projects onto the first baroclinic mode, it may play a similar role to the zonally symmetric geostrophic modes on coupling first baroclinic structure equatorial waves and barotropic Rossby waves. The coupling with boundary layer can also have some effects on the resonances explored in this paper, due to the change in the bottom boundary condition. The authors also intend to investigate these issues in the future.

Other requirements for the application of the present theory to the real atmosphere are the inclusion of the dynamical effects of the spherical geometry and the extension of the vertical domain adopted here to allow the coupling with the stratosphere because the equatorial waves typically observed in the atmosphere have a significant stratospheric extension (Wheeler et al. 2000). The stratospheric extension of the vertical domain adopted in this paper requires the use of a more realistic vertical stratification of the background atmosphere. Silva Dias and Bonatti (1986) have computed the vertical eigenmodes of a primitive equation atmospheric model by using a temperature vertical profile obtained from observational data of the First Global Atmosphere Research Program (GARP) Global Experiment (FGGE) level III-b to analyze the sensitivity of the vertical mode expansion to the vertical resolution of the model. Besides the vertical eigenmodes obtained in this work (Table 1), Silva Dias and Bonatti obtained other modes characterized by gravity wave speeds of 178.3, 91.4, 62.0, 28.3, and 15.75 m s^{-1}. Thus, considering a more realistic stratification of the background atmosphere, more vertical eigenmodes are allowed. This suggests that resonant triad interactions in the real atmosphere might be even more favored than indicated in this theoretical study.

Acknowledgments. The work presented in this paper was part of the first author's doctoral thesis developed at the University of São Paulo. This thesis was financially supported by FAPESP (Fundação de Amparo à Pesquisa do Estado de São Paulo) under Grant 02/09683-9. We also acknowledge the support from PROSUR/IRI and the Moore Foundation. The work of P. Milewski and E. G. Tabak was partially supported by grants from the applied mathematical division of NSF. We would also like to thank the anonymous reviewers for their useful suggestions to improve this manuscript.

REFERENCES

Abramowitz, M., and I. A. Stegun, Eds., 1964: *Handbook of Mathematical Functions*. Dover, 1046 pp.

Bretherton, F. P., 1964: Resonant interactions between waves. The case of discrete oscillations. *J. Fluid Mech.,* **20,** 457–479.

Case, K. M., and S. C. Chiu, 1977: Three-wave resonant interactions of gravity–capillary waves. *Phys. Fluids,* **20,** 742–745.

Craik, A. D. D., 1985: *Wave Interactions and Fluid Flows.* Cambridge University Press, 322 pp.

DeMaria, M., 1985: Linear response of a stratified tropical atmosphere to convective forcing. *J. Atmos. Sci.,* **42,** 1944–1959.

Domaracki, A., and A. Z. Loesch, 1977: Nonlinear interactions among equatorial waves. *J. Atmos. Sci.,* **34,** 486–498.

Haertel, P. T., and G. Kiladis, 2004: Dynamics of 2-day equatorial waves. *J. Atmos. Sci.,* **61,** 2707–2721.

Hoskins, B. J., and D. J. Karoly, 1981: The steady linear response of a spherical atmosphere to thermal and orographic forcing. *J. Atmos. Sci.,* **38,** 1179–1196.

Kasahara, A., and P. L. Silva Dias, 1986: Response of planetary waves to stationary tropical heating in a global atmosphere with meridional and vertical shear. *J. Atmos. Sci.,* **43,** 1893–1911.

Lindzen, R. S., 1967: Planetary waves on beta-planes. *Mon. Wea. Rev.,* **95,** 441–451.

Loesch, A. Z., and R. C. Deininger, 1979: Dynamics of closed systems of resonantly interacting equatorial waves. *J. Atmos. Sci.,* **36,** 1490–1497.

Lorenz, E. N., 1963: The mechanics of vacillation. *J. Atmos. Sci.,* **20,** 448–464.

Matsuno, T., 1966: Quasi-geostrophic motions in the equatorial area. *J. Meteor. Soc. Japan,* **44,** 25–43.

McGoldrick, L. F., 1965: Resonant interactions among capillary–gravity waves. *J. Fluid Mech.,* **21,** 305–331.

Milewski, P., and J. B. Keller, 1996: Three-dimensional water waves. *Stud. Appl. Math.,* **97,** 149–166.

Phillips, O. M., 1960: On the dynamics of unsteady gravity waves of finite amplitude. Part 1. The elementary interactions. *J. Fluid Mech.,* **9,** 193–217.

Raupp, C. F. M., and P. L. Silva Dias, 2006: Dynamics of resonantly interacting equatorial waves. *Tellus,* **58A,** 263–279.

Ripa, P., 1981: On the theory of nonlinear wave–wave interactions among geophysical waves. *J. Fluid Mech.,* **103,** 87–115.

——, 1982: Nonlinear wave–wave interactions in a one-layer reduced-gravity model on the equatorial β plane. *J. Phys. Oceanogr.,* **12,** 97–111.

——, 1983a: Weak interactions of equatorial waves in a one-layer model. Part I: General properties. *J. Phys. Oceanogr.,* **13,** 1208–1226.

——, 1983b: Weak interactions of equatorial waves in a one-layer model. Part II: Applications. *J. Phys. Oceanogr.,* **13,** 1227–1240.

Silva Dias, P. L., and W. H. Schubert, 1979: The dynamics of equatorial mass-flow adjustment. Atmospheric Science Paper 312, Department of Atmospheric Science, Colorado State University, 312 pp.

——, and J. P. Bonatti, 1985: A preliminary study of the observed vertical mode structure of the summer circulation over tropical South America. *Tellus,* **37A,** 185–195.

——, and ——, 1986: Vertical mode decomposition and model resolution. *Tellus,* **38A,** 205–214.

——, W. H. Schubert, and M. DeMaria, 1983: Large-scale response of the tropical atmosphere to transient convection. *J. Atmos. Sci.,* **40,** 2689–2707.

Wheeler, M., G. N. Kiladis, and P. J. Webster, 2000: Large-scale dynamical fields associated with convectively coupled equatorial waves. *J. Atmos. Sci.,* **57,** 613–640.